

1    **Title**

2    Hippocampus and amygdala fear memory engrams re-emerge after contextual fear reinstatement

3    **Authors**

4    Yosif Zaki<sup>1,3</sup>, William Mau<sup>1,3</sup>, Christine Cincotta<sup>2</sup>, Anahita Hamidi<sup>2</sup>, Emily Doucette<sup>2</sup>, Stephanie  
5    L. Grella<sup>2</sup>, Emily Merfeld<sup>2</sup>, Nathen J. Murawski<sup>2</sup>, Monika Shpokayte<sup>2</sup>, Steve Ramirez<sup>2,4,\*</sup>.

6    <sup>1</sup>Department of Neuroscience, School of Medicine at Mount Sinai, New York, NY, 10029

7    <sup>2</sup>Department of Psychological and Brain Sciences, Boston University, Boston, MA, 02215

8    <sup>3</sup>These authors contributed equally to this work

9    <sup>4</sup>Lead Contact

10   \*Correspondence: [dvsteve@bu.edu](mailto:dvsteve@bu.edu)

11   **Abstract**

12   The formation and extinction of fear memories represent two forms of learning that each  
13   engage the hippocampus and amygdala. How cell populations in these areas contribute to fear  
14   relapse, however, remains unclear. Here, we demonstrate that, in mice, cells active during fear  
15   conditioning in the dentate gyrus of hippocampus and basolateral amygdala exhibit decreased  
16   activity during extinction and are re-engaged after fear reinstatement. *In vivo* calcium imaging  
17   reveals that reinstatement drives population dynamics in the basolateral amygdala to revert to a  
18   network state similar to the state present during fear conditioning. Finally, we find that  
19   optogenetic inactivation of neuronal ensembles active during fear conditioning in either the  
20   hippocampus or amygdala is sufficient to disrupt fear expression after reinstatement. These  
21   results suggest that fear reinstatement triggers a partial re-emergence of the original fear memory  
22   representation, providing new insight into the neural substrates of fear relapse.

23   **Introduction**

24   The biological capacity to produce adaptive behavioral responses in actively changing  
25   environments is critical to an animal's survival. Contextual fear conditioning (CFC) is a form of  
26   learning whereby an animal learns to associate a conditioned stimulus (e.g. a context) with an  
27   unconditioned aversive stimulus (e.g. foot shocks) to produce a conditioned response to the  
28   conditioned stimulus (e.g. freezing). Conditioned responses can be mitigated through extinction  
29   learning via repeated exposure to the conditioned context in the absence of the foot shock.  
30   However, while extinction learning can be effective at attenuating fear, animals are susceptible  
31   to fear relapse under several conditions, including exposure to stressors, the passage of time, and  
32   re-exposure to the unconditioned stimulus (Goode, Jin, & Maren, 2018). This observation in  
33   rodents shares numerous similarities to clinical observations: exposure therapy – a clinical  
34   analog to extinction learning – can be effective at reducing fear in subsets of patients with  
35   anxiety disorders or post-traumatic stress disorder. However, many patients are still susceptible  
36   to fear relapse following successful exposure therapy (Kearns, Ressler, Zatzick, & Rothbaum,  
37   2012). Despite an extensive body of literature investigating the neural substrates of fear and  
38   extinction learning (Maren, 2001), how discrete neuronal populations causally contribute to fear  
39   relapse remains incompletely understood.

40   Previous studies have demonstrated that cells in the dorsal dentate gyrus of the  
41   hippocampus (DG) and in the basolateral amygdala (BLA) that are active during fear  
42   conditioning (hereafter referred to as the DG and BLA fear ensembles) are preferentially re-

47 activated during fear memory recall (Ramirez et al., 2013; Reijmers, Perkins, Matsuo, &  
48 Mayford, 2007), and are necessary and sufficient for the expression of defensive behaviors such  
49 as freezing (Denny et al., 2014; Redondo et al., 2014). Additionally, recent evidence has  
50 indicated that extinction learning may be mediated by interactions between local BLA  
51 interneurons and a BLA fear ensemble (Davis, Zaki, Maguire, & Reijmers, 2017), while a new  
52 set of cells simultaneously emerges in both the hippocampus (Khalaf et al., 2018; Lacagnina et  
53 al., 2019; Tronson et al., 2009) and BLA (Herry et al., 2008), possibly to encode extinction  
54 learning. However, whether fear relapse re-engages the original memory-encoding neuronal  
55 population or gives rise to a new representation remains unclear.  
56

## 57 Results

58 To address this, we first developed a behavioral protocol for fear reinstatement, a model  
59 of fear relapse in rodents (Rescorla & Heth, 1975). Mice underwent CFC and two subsequent  
60 extinction (EXT) sessions over two days, followed by an immediate shock (IS) in a novel context  
61 to reinstate the original fear memory, and a post-reinstatement recall test (IS-Recall) the  
62 following day to measure the return of fear (Figure 1a, bottom behavioral schedule).  
63 Reinstatement led to an increase in freezing in the original conditioned context (Figure 1—figure  
64 supplement 1a-e) and was largely context specific (Figure 1—figure supplement 2a,b).

65 Next, we determined if the cells active during fear conditioning were preferentially re-  
66 activated after mice underwent extinction and subsequent reinstatement. To that end, we tagged  
67 cells active during fear conditioning by injecting an activity-dependent viral cocktail of AAV9-c-  
68 Fos-tTA and AAV9-TRE-eYFP in the DG and BLA of adult male mice (Figure 1b,c). This virus  
69 enabled expression of eYFP in cells sufficiently active to express the immediate early gene c-  
70 Fos, which is under the repressive control of the antibiotic doxycycline (DOX)(Reijmers et al.,  
71 2007). We then measured immunoreactive c-Fos and calculated overlap between the set of cells  
72 active during CFC (eYFP-expressing cells) and during different stages of the behavioral schedule  
73 (c-Fos-expressing cells) (Figure 1d,e).

74 Previous reports have shown that the number of BLA cells active during both fear  
75 conditioning and fear memory recall correlates with freezing levels (Reijmers et al., 2007). Thus,  
76 we reasoned that if reinstatement re-engages the fear ensemble, the set of cells active during fear  
77 conditioning would be active again following reinstatement, and freezing during recall would  
78 correlate with cellular overlap. We found that, as expected, cells active during CFC were highly  
79 re-activated during Recall the following day, and EXT led to a modest, non-significant decrease  
80 in overlap. Interestingly, compared to EXT-Recall, mice exhibited more overlap in the BLA after  
81 reinstatement during a post-reinstatement recall session (IS-Recall) (Figure 1f). However,  
82 freezing behavior during Recall sessions did not correlate with BLA fear ensemble re-activation  
83 across the FC-Recall, EXT-Recall, and IS-Recall groups, indicating that BLA fear ensemble  
84 activity may not be predictive of freezing across these behavioral conditions (Figure 1g). The IS-  
85 Recall group exhibited greater overall expression of cFos than the EXT-Recall group, but less  
86 overall expression of eYFP than the EXT-Recall group; overall expression of cFos and eYFP  
87 was otherwise stable across groups (Figure 1—figure supplement 1f,g).

88 In the DG, we similarly observed significant overlap between the set of cells active  
89 during CFC and cells active during fear memory recall, as previously reported (Ramirez et al.,  
90 2013) (Figure 1h). In support of the notion that the dorsal DG processes changes in  
91 environmental contingencies (Fanselow & Dong, 2010), this overlap substantially decreased  
92 after EXT. While overlap remained low after IS, it significantly increased when mice were given

93 the IS and were placed back into the original conditioned context the following day, suggesting  
94 that fear reinstatement may re-engage the set of cells originally active during fear conditioning  
95 (Figure 1h). Additionally, unlike BLA overlaps, freezing behavior correlated with overlaps in the  
96 DG across all groups (Figure 1i), indicating that DG fear ensemble re-activation was predictive  
97 of freezing. Overall expression of eYFP and cFos was stable across groups in DG (Figure 1—  
98 figure supplement 1h,i).

99 Whereas our c-Fos-based labeling system allowed comparisons between activity of cells  
100 across two discrete timepoints with high spatial resolution, it was incapable of measuring activity  
101 at finer timescales due to the slow kinetics of immediate-early gene expression relative to real-  
102 time neural activity. To overcome this weakness, we next utilized an *in vivo* calcium ( $\text{Ca}^{2+}$ )  
103 imaging approach to record real-time neuronal activity in the BLA in freely moving mice during  
104 exposures to both a conditioned context and a neutral context where no shocks were delivered  
105 (Figure 2a-b). We tracked these cells longitudinally over the course of the reinstatement  
106 schedule, in order to determine whether shared population dynamics are associated with both  
107 fear conditioning and reinstatement (Sheintuch et al., 2017) (Figure 2c; see also Figure 2—figure  
108 supplement 2). To define initial population states, we constructed  $\text{Ca}^{2+}$  transient rate population  
109 vectors from the CFC session for each mouse. Then, to compare extinction and post-  
110 reinstatement recall states to CFC, we correlated population vectors from EXT and Recall (in 30  
111 s non-overlapping time windows) to the CFC population vector. We found that over EXT, the  
112 population states in the BLA gradually deviated from its state during CFC, supporting the idea of  
113 a network-wide transformation over extinction (Grewe et al., 2017; Hartley et al., 2019; Herry et  
114 al., 2008; Tronson et al., 2009) (Figure 2d). However, during Recall, the BLA population  
115 rebounded towards the CFC network state to an extent greater than expected by chance (Figure  
116 2e, left). These effects were absent in a neutral context and in CA1 of hippocampus (Figure 2e,  
117 right; see also Figure 2—figure supplement 1), demonstrating that the conditioned context and  
118 BLA drove these dynamics. Next, using an algorithm for extracting co-active neurons from  
119 simultaneously recorded cells (Lopes-dos-Santos, Ribeiro, & Tort, 2013), we characterized  
120 neuronal ensembles that were highly active during individual sessions (CFC, EXT1, and EXT2).  
121 Then, during Recall, we correlated the activity of these ensembles to freezing and found that the  
122 activity of ensembles extracted during CFC and EXT1 reliably predicted relapse freezing, but the  
123 ensembles extracted during EXT2 did not (Figure 2f). No ensembles predicted freezing in the  
124 neutral context. This suggested that BLA activity patterns contributed to expression of fear  
125 relapse, but only before extinction training modified these patterns. Overall, these data indicated  
126 that context-specific reinstated fear was associated with the emergence of network states in the  
127 BLA that resembled network states during fear conditioning, suggesting that a relapsed fear  
128 memory may be represented by a similar trace as the original fear memory.

129 Finally, we sought to determine whether the activity of cells active during fear  
130 conditioning was necessary for expression of reinstated fear. To do this, we bilaterally injected  
131 mice in either the DG or the BLA with a virus cocktail of AAV9-c-Fos-tTA and AAV9-TRE-  
132 ArchT-eYFP to drive expression of the light-sensitive protein archaerhodopsin (ArchT) in cells  
133 active during CFC, and subsequently implanted optic fibers above the injection sites (Figure  
134 3a,b). Mice then underwent two EXT sessions, the reinstating shock, and recall the following day  
135 (Figure 3c). Mice in both the DG and BLA experimental groups showed significant suppression  
136 of freezing during optical inhibition. This manipulation was reversible, as freezing increased  
137 again in the following light-off epoch (Figure 3d,e). eYFP controls did not show this decrease in

138 freezing during optical inhibition, confirming that the behavioral effect was dependent on  
139 expression of ArchT (Figure 3f,g).

140 Since the BLA is widely acknowledged as a necessary hub for fear learning (Bocchio,  
141 Nabavi, & Capogna, 2017), we next probed whether activity of the BLA fear ensemble during  
142 the reinstating shock was necessary or sufficient to induce fear reinstatement. To test necessity,  
143 we adopted a similar approach as above in order to express ArchT selectively within the BLA  
144 fear ensemble, and then implanted optic fibers bilaterally above BLA (Figure 3—figure  
145 supplement 1a,b). Mice underwent FC and EXT, had the BLA fear ensemble inhibited during the  
146 reinstating shock, and were then returned to the original conditioned context to assess whether  
147 reinstatement could be prevented (Figure 3—figure supplement 1c,d). Surprisingly, mice that  
148 had the BLA fear ensemble inhibited did not freeze any less during post-reinstatement recall than  
149 eYFP controls (Figure 3—figure supplement 1e). To test sufficiency, we selectively expressed  
150 ChR2 in either the BLA fear ensemble or DG fear ensemble in separate groups of mice. Mice  
151 underwent FC and EXT, were then placed in a novel chamber, and rather than receiving the  
152 reinstating shock, mice had either the BLA or DG fear ensemble stimulated for 60 seconds. The  
153 next day, they were placed back in the original conditioned context to assess whether the  
154 stimulation could mimic reinstatement (Figure 3—figure supplement 2a-c). Mice that had the  
155 BLA fear ensemble stimulated froze no more than eYFP controls (Figure 3—figure supplement  
156 2d), while mice that had the DG fear ensemble stimulated only showed modest, non-significant  
157 increases in freezing relative to the eYFP controls (Figure 3—figure supplement 2e). These  
158 results indicated that despite a crucial role for the BLA and DG fear ensembles in fear learning,  
159 activity of these populations was not sufficient to drive fear reinstatement, and activity of the  
160 BLA population was not necessary to drive reinstatement either.

161 To test whether the functional role for these cells emerged only after reinstatement or if  
162 inhibition of the fear ensemble could suppress freezing during extinction, we inhibited the DG or  
163 BLA fear ensemble during an extinction recall session—when low levels of freezing were still  
164 present—and observed that inhibition of the DG fear ensemble led to a mild reduction in  
165 freezing, while inhibition of the BLA fear ensemble did not disrupt freezing (Figure 3—figure  
166 supplement 3). These results suggested that extinction differentially modified the BLA and DG  
167 fear ensembles, such that BLA ensemble inhibition did not disrupt freezing during extinction,  
168 while DG ensemble activity may have been actively involved in contextual fear expression  
169 during extinction.

170 We next determined whether nonspecific manipulation of DG or BLA cells could reduce  
171 freezing responses, as opposed to being driven specifically by the fear ensemble in these regions.  
172 We tagged cells either in the DG or the BLA that were active during female exposure—an  
173 unrelated experience of opposing valence, which has previously been shown to label similar  
174 proportions of neurons in both the DG and BLA (Chen et al., 2019; Ramirez et al., 2013;  
175 Redondo et al., 2014)—and inhibited those cells during post-reinstatement recall (Figure 3h).  
176 Interestingly, whereas this manipulation in the BLA did not cause behavioral changes, inhibition  
177 of non-fear cells in the DG led to a modest light-induced reduction in freezing (Figure 3i,j).  
178 These results are consistent with the notion that perturbing DG dynamics can produce a general  
179 modulation of freezing responses, while only inhibition of BLA fear cells directly disrupts  
180 freezing per se. Difference scores between freezing during light-on vs light-off epochs revealed  
181 that inhibition of DG fear cells led to moderately less freezing during light-on epochs compared  
182 to eYFP controls (Figure 3k), while inhibition of BLA fear cells led to significantly less freezing  
183 during light-on epochs (Figure 3l). Finally, one-sample z-tests on difference scores revealed that

184 only mice that had the fear ensemble inhibited (experimental groups; Exp) froze significantly  
185 less during light-on epochs than light-off epochs, whereas mice that had female exposure cells  
186 inhibited (positive; Pos) and eYFP control mice (eYFP) froze no differently during light-on and  
187 light-off epochs (Figure 3m).

188

## 189 Discussion

190 The dynamic nature of fear memory expression constitutes a difficult problem for  
191 mitigating fear in the clinic: patients with fear-related disorders who have undergone successful  
192 treatment are still prone to relapse, and the underlying causal mechanisms facilitating fear  
193 reinstatement are largely unknown. A commonly held view is that fear extinction is not an  
194 unlearning of the original trauma; rather, a second memory develops that suppresses the original  
195 aversive memory. This raises an important notion about the nature of the ensemble regulating  
196 fear expression post-reinstatement. One idea is that the original ensemble driving fear expression  
197 and a new ensemble driving fear suppression actively compete to influence behavioral output.  
198 Under this framework, fear relapse could be the result of the fear ensemble dominating.  
199 Alternatively, fear relapse might be driven by recruitment of a new, discrete cellular population  
200 that does not involve the original fear ensemble. A likely scenario is a mixture of the two, where  
201 fear relapse materializes from a partial re-emergence of the original ensemble in parallel with  
202 recruitment of new neuronal connections (Clem & Schiller, 2016), which our c-Fos labeling,  
203 Ca<sup>2+</sup> imaging, and optogenetics evidence collectively support.

204 Ca<sup>2+</sup> imaging and c-Fos labeling during the fear reinstatement schedule enabled us to  
205 capture network dynamics from the hippocampus and amygdala over multiple timescales,  
206 shedding light on the activity of these regions over fear reinstatement. Consistent with prior  
207 reports of BLA cell populations up- and down-regulating their activity during extinction learning  
208 (Grewe et al., 2017; Herry et al., 2008), and with immediate-early gene data presented here, we  
209 observed decorrelation of the BLA population vector from the initial fear-encoding state over  
210 repeated exposures to the conditioned context. This time-dependent transformation has  
211 previously been depicted in numerous brain regions as “representational drift” (Driscoll, Pettit,  
212 Minderer, Chettih, & Harvey, 2017; Mankin et al., 2012; Mau et al., 2018; Rubin, Geva,  
213 Sheintuch, & Ziv, 2015; Rule, O’Leary, & Harvey, 2019), but these studies all described  
214 population states that monotonically drifted *away* from a reference session. In the present study,  
215 the BLA representation exhibited similar dynamics, but in contrast to past work, regressed its  
216 neural trajectory *back towards* the initial representation after fear reinstatement. This leads us to  
217 believe that fear reinstatement may be restoring a remote memory trace similar to how related  
218 optogenetic studies artificially induce memory retrieval (Liu et al., 2012; Ramirez et al., 2013;  
219 Redondo et al., 2014).

220 Interestingly, the neural patterns associated with fear expression are still retrievable after  
221 putative circuit remodeling over extinction learning and fear reinstatement (Bocchio et al., 2017;  
222 Davis et al., 2017; Hartley et al., 2019; Maren, 2015). Our ability to observe and manipulate the  
223 original fear ensemble after reinstatement is suggestive of a latent representation of the original  
224 memory that persists and coexists with the newly formed extinction memory (Lacagnina et al.,  
225 2019; Maren, 2011). However, this new extinction memory may also facilitate local synaptic  
226 remodeling that modifies the original fear memory, which may explain why inhibition of the fear  
227 ensemble in DG and BLA did not fully eliminate freezing. The re-emergence of the original fear  
228 memory may also depend on strict plasticity mechanisms, which can explain why we failed to  
229 optically induce relapse through broad stimulation of the BLA fear ensemble after extinction

230 (Figure 3—figure supplement 2). These results suggest that the natural endogenous fear  
231 reinstatement process might require certain activity patterns for modifying the original fear  
232 ensemble that could not be artificially produced through BLA stimulation alone. For example,  
233 recent work showed that sequential activity from triplets of BLA neurons preceded fear learning  
234 (Reitich-Stolero & Paz, 2019) and similar patterns may underlie fear reinstatement. Fear  
235 reinstatement may then be recruiting a subset of the original fear ensemble while forming new  
236 synaptic linkages with a novel cell population. Others have shown that unique memories reside  
237 in patterns of connectivity between memory-encoding – or engram – cells in the hippocampal  
238 system (Abdou et al., 2018; Ryan, Roy, Pignatelli, Arons, & Tonegawa, 2015; Tonegawa,  
239 Morrissey, & Kitamura, 2018). In the context of our study, reinstatement could be modifying  
240 these functional linkages to engage a new set of engram cells, possibly those that are highly  
241 excitable at the time of the experience (Cai et al., 2016; Rashid et al., 2016; Yiu et al., 2014),  
242 forming a reinstatement ensemble that is similar, but not identical, to the original fear ensemble.  
243 In accordance with this idea, post-reinstatement recall activates a large proportion, but not all, of  
244 the original fear ensemble (Figure 1f,h).

245 While our optogenetic experiments suggest a re-emergence of the fear ensemble in the  
246 DG, we were unable to perform calcium imaging in DG due to the technical limitations of  
247 accessing this region without significant damage to overlying hippocampal subareas.  
248 Nonetheless, we report that CA1 exhibits only marginally significant ( $p = 0.075$ , Figure 2—  
249 figure supplement 1b) reversion of calcium dynamics to a fear conditioning-like state after  
250 reinstatement. This may be due to the functional differences between DG and CA1, with CA1  
251 possibly responding to more contextual features of the experience (Tanaka et al., 2018) or being  
252 overall more subject to plasticity than DG. As others have found, day-to-day dynamics of spatial  
253 activity in DG are more stable than in CA1 (Hainmueller & Bartos, 2018). Until methods are  
254 developed that allow unfettered imaging of DG while still preserving superficial hippocampal  
255 areas, it remains unknown whether the real-time network activity of DG exhibit relapse-induced  
256 reactivation of fear ensembles. However, recent work agrees with our prediction that extinction  
257 suppresses fear-related activity in the DG while those activity patterns are retrieved during  
258 relapse (Lacagnina et al., 2019).

259 Further work exploring the competing interactions of cellular networks across fear  
260 learning and fear suppression could provide important insight into how the brain competes for  
261 the expression of fear throughout fear extinction and relapse. Moreover, a deeper understanding  
262 of how fear memories are modified by time and experience may help guide development of  
263 treatments for trauma-related disorders, and these findings point to hippocampal- and BLA-  
264 mediated engrams as key nodes contributing to the re-emergence of a contextual fear memory.

265  
266  
267  
268  
269  
270  
271  
272  
273  
274  
275

276 **Acknowledgements**

277 We thank Dr. Joshua Sanes and his lab at the Center for Brain Science, Harvard  
278 University, for providing laboratory space within which the initial experiments were conducted,  
279 the Center for Brain Science Neuroengineering core for providing technical support, and the  
280 Society of Fellows at Harvard University for their support. We also thank Dr. Susumu Tonegawa  
281 and his lab for providing the activity-dependent virus cocktail, Dr. Chris MacDonald for  
282 consultation on behavioral schedules, and Drs. Leon Reijmers and Patrick Davis, for their help  
283 with formulating this project and for their feedback throughout. We also thank Vardhan Dani and  
284 Inscopix for their technical assistance as well as Helen Fawcett and the NSF Neurophotonics  
285 Research Traineeship Program for funding and support. This work was supported by an NIH  
286 Early Independence Award (DP5 OD023106-01), an NIH Transformative R01 Award, a Young  
287 Investigator Grant from the Brain and Behavior Research Foundation, a Ludwig Family  
288 Foundation grant, and the McKnight Foundation Memory and Cognitive Disorders award.  
289  
290

291 **Author Contributions**

292 Y.Z. and S.R. conceived the study. Y.Z., W.M., and S.R. designed experiments and  
293 analyzed data. Y.Z., W.M., C.C., A.H., E.D., S.L.G., E.M., N.J.M., and M.S. conducted  
294 experiments. Y.Z., W.M., and S.R. wrote the manuscript; all authors edited and commented on  
295 the manuscript.  
296  
297

298 **Declaration of Interests**

299 The authors declare no competing interests.  
300  
301  
302  
303  
304  
305  
306  
307  
308  
309  
310  
311  
312  
313  
314  
315  
316  
317  
318  
319  
320  
321

- 322 **References**
- 323 Abdou, K., Shehata, M., Choko, K., Nishizono, H., Matsuo, M., Muramatsu, S. I., & Inokuchi,  
324 K. (2018). Synapse-specific representation of the identity of overlapping memory  
325 engrams. *Science*, 360(6394), 1227-1231. doi:10.1126/science.aat3810
- 326 Bocchio, M., Nabavi, S., & Capogna, M. (2017). Synaptic Plasticity, Engrams, and Network  
327 Oscillations in Amygdala Circuits for Storage and Retrieval of Emotional Memories.  
328 *Neuron*, 94(4), 731-743. doi:10.1016/j.neuron.2017.03.022
- 329 Cai, D. J., Aharoni, D., Shuman, T., Shobe, J., Biane, J., Song, W., . . . Silva, A. J. (2016). A  
330 shared neural ensemble links distinct contextual memories encoded close in time. *Nature*,  
331 534(7605), 115-118. doi:10.1038/nature17955
- 332 Chen, B. K., Murawski, N. J., Cincotta, C., McKissick, O., Finkelstein, A., Hamidi, A. B., . . .  
333 Ramirez, S. (2019). Artificially Enhancing and Suppressing Hippocampus-Mediated  
334 Memories. *Curr Biol*, 29(11), 1885-1894 e1884. doi:10.1016/j.cub.2019.04.065
- 335 Clem, R. L., & Schiller, D. (2016). New Learning and Unlearning: Strangers or Accomplices in  
336 Threat Memory Attenuation? *Trends Neurosci*, 39(5), 340-351.  
337 doi:10.1016/j.tins.2016.03.003
- 338 Davis, P., Zaki, Y., Maguire, J., & Reijmers, L. G. (2017). Cellular and oscillatory substrates of  
339 fear extinction learning. *Nat Neurosci*, 20(11), 1624-1633. doi:10.1038/nn.4651
- 340 Denny, C. A., Kheirbek, M. A., Alba, E. L., Tanaka, K. F., Brachman, R. A., Laughman, K. B., .  
341 . . Hen, R. (2014). Hippocampal memory traces are differentially modulated by  
342 experience, time, and adult neurogenesis. *Neuron*, 83(1), 189-201.  
343 doi:10.1016/j.neuron.2014.05.018
- 344 Driscoll, L. N., Pettit, N. L., Minderer, M., Chettih, S. N., & Harvey, C. D. (2017). Dynamic  
345 Reorganization of Neuronal Activity Patterns in Parietal Cortex. *Cell*, 170(5), 986-999  
346 e916. doi:10.1016/j.cell.2017.07.021
- 347 Fanselow, M. S., & Dong, H. W. (2010). Are the dorsal and ventral hippocampus functionally  
348 distinct structures? *Neuron*, 65(1), 7-19. doi:10.1016/j.neuron.2009.11.031
- 349 Goode, T. D., Jin, J., & Maren, S. (2018). 10 - Neural Circuits for Fear Relapse. In S. Sangha &  
350 D. Foti (Eds.), *Neurobiology of Abnormal Emotion and Motivated Behaviors* (pp. 182-  
351 202): Academic Press.
- 352 Grewe, B. F., Grundemann, J., Kitch, L. J., Lecoq, J. A., Parker, J. G., Marshall, J. D., . . .  
353 Schnitzer, M. J. (2017). Neural ensemble dynamics underlying a long-term associative  
354 memory. *Nature*, 543(7647), 670-675. doi:10.1038/nature21682
- 355 Hainmueller, T., & Bartos, M. (2018). Parallel emergence of stable and dynamic memory  
356 engrams in the hippocampus. *Nature*, 558(7709), 292-296. doi:10.1038/s41586-018-  
357 0191-2
- 358 Hartley, N. D., Gaulden, A. D., Baldi, R., Winters, N. D., Salimando, G. J., Rosas-Vidal, L. E., .  
359 . . Patel, S. (2019). Dynamic remodeling of a basolateral-to-central amygdala  
360 glutamatergic circuit across fear states. *Nat Neurosci*. doi:10.1038/s41593-019-0528-7
- 361 Herry, C., Ciocchi, S., Senn, V., Demmou, L., Muller, C., & Luthi, A. (2008). Switching on and  
362 off fear by distinct neuronal circuits. *Nature*, 454(7204), 600-606.  
363 doi:10.1038/nature07166
- 364 Kearns, M. C., Ressler, K. J., Zatzick, D., & Rothbaum, B. O. (2012). Early interventions for  
365 PTSD: a review. *Depress Anxiety*, 29(10), 833-842. doi:10.1002/da.21997

- 366 Khalaf, O., Resch, S., Dixsaut, L., Gorden, V., Glauser, L., & Graff, J. (2018). Reactivation of  
367 recall-induced neurons contributes to remote fear memory attenuation. *Science*,  
368 360(6394), 1239-1242. doi:10.1126/science.aas9875
- 369 Lacagnina, A. F., Brockway, E. T., Crovetti, C. R., Shue, F., McCarty, M. J., Sattler, K. P., . . .  
370 Drew, M. R. (2019). Distinct hippocampal engrams control extinction and relapse of fear  
371 memory. *Nat Neurosci*, 22(5), 753-761. doi:10.1038/s41593-019-0361-z
- 372 Liu, X., Ramirez, S., Pang, P. T., Puryear, C. B., Govindarajan, A., Deisseroth, K., & Tonegawa,  
373 S. (2012). Optogenetic stimulation of a hippocampal engram activates fear memory  
374 recall. *Nature*, 484(7394), 381-385. doi:10.1038/nature11028
- 375 Lopes-dos-Santos, V., Ribeiro, S., & Tort, A. B. (2013). Detecting cell assemblies in large  
376 neuronal populations. *J Neurosci Methods*, 220(2), 149-166.  
377 doi:10.1016/j.jneumeth.2013.04.010
- 378 Mankin, E. A., Sparks, F. T., Slayyeh, B., Sutherland, R. J., Leutgeb, S., & Leutgeb, J. K.  
379 (2012). Neuronal code for extended time in the hippocampus. *Proc Natl Acad Sci U S A*,  
380 109(47), 19462-19467. doi:10.1073/pnas.1214107109
- 381 Maren, S. (2001). Neurobiology of Pavlovian fear conditioning. *Annu Rev Neurosci*, 24, 897-  
382 931. doi:10.1146/annurev.neuro.24.1.897
- 383 Maren, S. (2011). Seeking a spotless mind: extinction, deconsolidation, and erasure of fear  
384 memory. *Neuron*, 70(5), 830-845. doi:10.1016/j.neuron.2011.04.023
- 385 Maren, S. (2015). Out with the old and in with the new: Synaptic mechanisms of extinction in  
386 the amygdala. *Brain Res*, 1621, 231-238. doi:10.1016/j.brainres.2014.10.010
- 387 Mau, W., Sullivan, D. W., Kinsky, N. R., Hasselmo, M. E., Howard, M. W., & Eichenbaum, H.  
388 (2018). The Same Hippocampal CA1 Population Simultaneously Codes Temporal  
389 Information over Multiple Timescales. *Curr Biol*, 28(10), 1499-1508 e1494.  
390 doi:10.1016/j.cub.2018.03.051
- 391 Mukamel, E. A., Nimmerjahn, A., & Schnitzer, M. J. (2009). Automated analysis of cellular  
392 signals from large-scale calcium imaging data. *Neuron*, 63(6), 747-760.  
393 doi:10.1016/j.neuron.2009.08.009
- 394 Ramirez, S., Liu, X., Lin, P. A., Suh, J., Pignatelli, M., Redondo, R. L., . . . Tonegawa, S. (2013).  
395 Creating a false memory in the hippocampus. *Science*, 341(6144), 387-391.  
396 doi:10.1126/science.1239073
- 397 Ramirez, S., Liu, X., MacDonald, C. J., Moffa, A., Zhou, J., Redondo, R. L., & Tonegawa, S.  
398 (2015). Activating positive memory engrams suppresses depression-like behaviour.  
399 *Nature*, 522(7556), 335-339. doi:10.1038/nature14514
- 400 Rashid, A. J., Yan, C., Mercaldo, V., Hsiang, H. L., Park, S., Cole, C. J., . . . Josselyn, S. A.  
401 (2016). Competition between engrams influences fear memory formation and recall.  
402 *Science*, 353(6297), 383-387. doi:10.1126/science.aaf0594
- 403 Redondo, R. L., Kim, J., Arons, A. L., Ramirez, S., Liu, X., & Tonegawa, S. (2014).  
404 Bidirectional switch of the valence associated with a hippocampal contextual memory  
405 engram. *Nature*, 513(7518), 426-430. doi:10.1038/nature13725
- 406 Reijmers, L. G., Perkins, B. L., Matsuo, N., & Mayford, M. (2007). Localization of a stable  
407 neural correlate of associative memory. *Science*, 317(5842), 1230-1233.  
408 doi:10.1126/science.1143839
- 409 Reitich-Stolero, T., & Paz, R. (2019). Affective memory rehearsal with temporal sequences in  
410 amygdala neurons. *Nat Neurosci*, 22(12), 2050-2059. doi:10.1038/s41593-019-0542-9

- 411 Rescorla, R. A., & Heth, C. D. (1975). Reinstatement of fear to an extinguished conditioned  
412 stimulus. *J Exp Psychol Anim Behav Process*, 1(1), 88-96.
- 413 Resendez, S. L., Jennings, J. H., Ung, R. L., Namboodiri, V. M., Zhou, Z. C., Otis, J. M., . . .  
414 Stuber, G. D. (2016). Visualization of cortical, subcortical and deep brain neural circuit  
415 dynamics during naturalistic mammalian behavior with head-mounted microscopes and  
416 chronically implanted lenses. *Nat Protoc*, 11(3), 566-597. doi:10.1038/nprot.2016.021
- 417 Rubin, A., Geva, N., Sheintuch, L., & Ziv, Y. (2015). Hippocampal ensemble dynamics  
418 timestamp events in long-term memory. *eLife*, 4. doi:10.7554/eLife.12247
- 419 Rule, M. E., O'Leary, T., & Harvey, C. D. (2019). Causes and consequences of representational  
420 drift. *Curr Opin Neurobiol*, 58, 141-147. doi:10.1016/j.conb.2019.08.005
- 421 Ryan, T. J., Roy, D. S., Pignatelli, M., Arons, A., & Tonegawa, S. (2015). Memory. Engram  
422 cells retain memory under retrograde amnesia. *Science*, 348(6238), 1007-1013.  
423 doi:10.1126/science.aaa5542
- 424 Sheintuch, L., Rubin, A., Brande-Eilat, N., Geva, N., Sadeh, N., Pinchasof, O., & Ziv, Y. (2017).  
425 Tracking the Same Neurons across Multiple Days in Ca(2+) Imaging Data. *Cell Rep*,  
426 21(4), 1102-1115. doi:10.1016/j.celrep.2017.10.013
- 427 Tanaka, K. Z., He, H., Tomar, A., Niisato, K., Huang, A. J. Y., & McHugh, T. J. (2018). The  
428 hippocampal engram maps experience but not place. *Science*, 361(6400), 392-397.  
429 doi:10.1126/science.aat5397
- 430 Tonegawa, S., Morrissey, M. D., & Kitamura, T. (2018). The role of engram cells in the systems  
431 consolidation of memory. *Nat Rev Neurosci*, 19(8), 485-498. doi:10.1038/s41583-018-  
432 0031-2
- 433 Tronson, N. C., Schrick, C., Guzman, Y. F., Huh, K. H., Srivastava, D. P., Penzes, P., . . .  
434 Radulovic, J. (2009). Segregated populations of hippocampal principal CA1 neurons  
435 mediating conditioning and extinction of contextual fear. *J Neurosci*, 29(11), 3387-3394.  
436 doi:10.1523/JNEUROSCI.5619-08.2009
- 437 Yiu, A. P., Mercaldo, V., Yan, C., Richards, B., Rashid, A. J., Hsiang, H. L., . . . Josselyn, S. A.  
438 (2014). Neurons are recruited to a memory trace based on relative neuronal excitability  
439 immediately before training. *Neuron*, 83(3), 722-735. doi:10.1016/j.neuron.2014.07.017
- 440
- 441
- 442
- 443
- 444
- 445
- 446
- 447
- 448
- 449
- 450
- 451
- 452
- 453
- 454
- 455
- 456

457 **Figure Legends**

458  
459 **Figure 1.** Histological characterization of fear reinstatement schedule. (a) Behavioral design for  
460 fear reinstatement. Mice underwent fear conditioning, and were then sacrificed at different points  
461 in the behavioral schedule and had tissue stained for c-Fos. (b) Schematic of viral strategy. A  
462 viral cocktail of AAV9-c-Fos-tTA and AAV9-TRE-eYFP was infused into the DG and BLA for  
463 activity-dependent induction of eYFP. (c) Representative microscope image for the injection  
464 sites. (d) Example confocal images of DG sections. Images from left to right: virus-labeled cells  
465 (eYFP), c-Fos<sup>+</sup> cells (cFos), merged green and red channels (Merge). Yellow arrows designate  
466 double-positive cells. Top images are representative of high overlap, and bottom are  
467 representative of low overlap. (e) Same as d but for BLA sections. (f) Quantitative analysis of  
468 overlap between FC-tagged BLA cells and c-Fos<sup>+</sup> BLA cells in each group. Overlap between  
469 FC-tagged cells and c-Fos<sup>+</sup> cells was high after FC and there was a trending decrease following  
470 EXT. Overlap remained low during the reinstating shock, but significantly increased during  
471 Recall after reinstatement. (n = 15-27 sections per group, i.e. 5 mice per group and 2-11 sections  
472 per mouse; F<sub>3,88</sub> = 5.25; one-way ANOVA followed by Tukey's post-hoc test for pairwise  
473 comparisons; #P < 0.1, \*P < 0.05, \*\*P < 0.01). Counts were normalized to % of eYFP<sup>+</sup> cells that  
474 were also c-Fos<sup>+</sup>. Small grey data points represent counts per section; big green data points  
475 represent average counts per animal for (f,h). (g) Correlation between average freezing during  
476 Recall and overlap in the BLA demonstrates that overlap in the BLA is not predictive of freezing  
477 (n = 15 mice; F<sub>1,13</sub> = 0.0209; ns P = 0.8873; R<sup>2</sup> = 0.0016; correlation). (h) Same as  
478 quantification in f, but for DG. Overlap between FC-tagged cells and c-Fos<sup>+</sup> cells was high after  
479 FC and significantly decreased following EXT. While overlap remained low during the  
480 reinstating shock, it significantly increased during Recall after reinstatement. (n = 18-27 sections  
481 per group, i.e. 4-6 mice and 2-6 sections per mouse; F<sub>3,89</sub> = 18.72; one-way ANOVA followed by  
482 Tukey's post-hoc test for pairwise comparisons; \*\*P < 0.01, \*\*\*P < 0.0001). (i) Correlation  
483 between average freezing during Recall and overlap in the DG demonstrates that overlap in the  
484 DG is predictive of freezing (n = 15 mice; F<sub>1,13</sub> = 6.374; \*P = 0.0254; R<sup>2</sup> = 0.329; correlation).  
485

486 **Figure 1 – figure supplement 1.** Behavior in reinstatement paradigm. (a) Mice underwent an 8-  
487 minute fear conditioning session (FC), with four 1.5mA shocks spaced 80-seconds apart.  
488 Compared to the first 3 minutes of FC (baseline freezing), mice froze significantly more in the  
489 first three minutes of the EXT1 session ( $t_{15} = 11.858$ , \*\*\*P < 0.0001; paired t-test; n = 16  
490 mice). (b) Mice underwent two 30-minute extinction sessions (EXT1 and EXT2) spaced 24  
491 hours apart. Mice spent significantly less time freezing in the last three minutes of EXT2 as  
492 compared to the first three minutes of EXT1 ( $t_{15} = 4.1631$ , \*\*\*P = 0.0008; paired t-test; n = 16  
493 mice). (c) Following EXT, one group of mice was returned to the conditioned context for Recall  
494 (EXT-Recall), while another group received an immediate shock in a novel context and was  
495 removed 60-seconds later. After 24 hours, those mice were tested in the original conditioned  
496 context for reinstatement (IS-Recall). (d) Compared to mice that did not receive the reinstating  
497 shock, those that did showed significantly more freezing across a 5-minute Recall session ( $t_8 =$   
498 4.631, \*\*P = 0.0017; unpaired t-test; n = 5 minutes for each group). (e) On average, mice that  
499 received the reinstating shock froze significantly more during Recall than did mice that did not  
500 receive the reinstating shock ( $t_6 = 4.018$ , \*\*P = 0.0070; unpaired t-test; n = 4 mice per group). (f)  
501 Quantification of relative numbers of eYFP<sup>+</sup> cells across groups in the BLA (calculated as  
502 #eYFP<sup>+</sup> cells divided by area in arbitrary units). The EXT-Recall group had greater numbers of

503 eYFP+ cells in the BLA than the IS group did ( $n = 15\text{-}27$  sections per group, i.e. 5 mice per  
504 group and 2-11 sections per mouse;  $F_{3,88} = 3.777$ ; one-way ANOVA followed by Tukey's post-  
505 hoc test for pairwise comparisons;  $\#P < 0.1$ ,  $*P < 0.05$ ). Small grey data points represent counts  
506 per section; big green data points represent average counts per animal for (f-i). (g) Quantification  
507 of relative numbers of cFos+ cells across groups in the BLA (calculated as \$cFos+ cells divided  
508 by area in arbitrary units). The IS-Recall group expressed greater numbers of cFos+ cells than  
509 did the EXT-Recall and IS groups ( $n = 15\text{-}27$  sections per group, i.e. 5 mice per group and 2-11  
510 sections per mouse;  $F_{3,88} = 3.444$ ; one-way ANOVA followed by Tukey's post-hoc test for  
511 pairwise comparisons;  $*P < 0.05$ ). (h) Same as (f) but for DG. The IS group had greater relative  
512 expression of eYFP+ cells than the the EXT-Recall group ( $n = 18\text{-}27$  sections per group, i.e. 4-6  
513 mice and 2-6 sections per mouse;  $F_{3,89} = 2.814$ ; one-way ANOVA followed by Tukey's post-hoc  
514 test for pairwise comparisons;  $*P < 0.05$ ). (i) Same as (g) but in DG. Expression of cFos+ cells in  
515 the DG was stable across all groups ( $n = 18\text{-}27$  sections per group, i.e. 4-6 mice and 2-6 sections  
516 per mouse;  $F_{3,89} = 1.216$ ; one-way ANOVA).

517

518 **Figure 1 – figure supplement 2.** Reinstatement leads to partial generalization, but is largely  
519 context-specific. (a) Behavioral design. Mice underwent the reinstatement as described in Figure  
520 1; however, they were placed in the original conditioned context (context A) and a novel context  
521 (context B), with some mice going into context A first and others context B first. (b) Compared  
522 to freezing in the novel context, mice froze significantly more in the original conditioned context  
523 across the 5-minute session ( $t_8 = 3.415$ ,  $**P = 0.0092$ ; unpaired t-test;  $n = 5$  minutes for each  
524 group).

525

526 **Figure 2.** BLA activity patterns change over extinction but resemble the fear conditioning state  
527 during fear relapse. (a) Behavioral schedule for  $\text{Ca}^{2+}$  imaging cohort. (b) Left, freezing time  
528 course of fear reinstatement paradigm ( $n = 6$  mice). Right, pooled freezing. EXT1 vs. EXT2,  
529 Wilcoxon signed-rank test  $p = 0.028$ ; EXT2 vs Recall  $p = 0.046$ . Data are means  $\pm$  standard error  
530 of the mean. (c) Left, example field of view in BLA-implanted mouse, depicted as maximum  
531 projection of CFC imaging session. Blue outlines indicate cell masks. Scale bar = 100 microns.  
532 Right, fluorescence traces of 10 example cells (d) Pearson correlation coefficients between  
533 population vectors during CFC and population vectors during EXT and Recall ( $n = 6$  mice). Each  
534 data point represents a measure of population similarity to CFC (30 s time bins). Two piecewise  
535 regressions were fit each to EXT and Recall. (e) Box plots of population vector similarity  
536 (predicted and empirical). Each data point represents a mouse's predicted r value (from the EXT  
537 regression) for Recall compared to the actual observed r value during Recall (Shock context,  
538 Wilcoxon signed-rank test  $p = 0.028$ ; Neutral context,  $p = 0.46$ ). (f) Groupings of neurons  
539 (ensembles) were extracted from CFC, EXT1, and EXT2 using a previously published PCA/ICA  
540 method (Lopes-dos-Santos et al., 2013). Averaged activations of those ensembles during Recall  
541 were correlated with freezing during Recall (CFC ensemble during Recall, Pearson correlation  $p$   
542 = 0.007; EXT1 ensemble during Recall  $p = 0.04$ ; EXT2 ensemble during Recall  $p = 0.80$ ).

543

544 **Figure 2 – figure supplement 1.** Reemergence of CFC-associated brain activity during fear  
545 relapse is specific to BLA and the shock context. (a) Left, correlation coefficients between EXT-  
546 Recall and CFC population vectors in the shock context for BLA ( $n = 6$  mice, duplicated from  
547 Figure 2d). Right, predicted vs. empirical correlation values during Recall (duplicated from  
548 Figure 2e). (b) Same as (a), but for CA1 ( $n = 6$  mice). (c) Same as (a), but for the neutral context

549 ( $n = 4$  mice). (d) Same as (c), but for CA1 ( $n = 4$  mice). Wilcoxon signed-rank tests  $p = 0.028$ ,  
550 0.075, 0.46, 0.46 for a-d respectively.  
551

552 **Figure 2 – figure supplement 2.** Cell registration examples. (a) Registration diagnostics for  
553 example CA1  $\text{Ca}^{2+}$  imaging mouse. Top, cell centroids pre-alignment. Middle, cell centroids  
554 post-alignment. Colors correspond to different sessions. Bottom, 2-dimensional histogram of  
555 matched pairs. Note the high density of cells within 3 microns of their match on another session.  
556 (b) Same as (a), but for example BLA mouse. Figures were modified from plots generated via  
557 software from Sheintuch et al., 2017.  
558

559 **Figure 3.** Optical inhibition of the DG or BLA fear ensemble disrupts reinstated fear. (a)  
560 Schematic of viral strategy. A virus cocktail of AAV9-c-Fos-tTA and AAV9-TRE-ArchT-eYFP  
561 was infused into either the DG or BLA for activity-dependent expression of ArchT-eYFP. (b)  
562 Representative microscope images of injection sites for the DG and BLA groups of mice. (c)  
563 Reinstatement behavioral schedule. Mice had the fear ensemble labeled in either the DG or BLA  
564 and inhibited during Recall after Shock Reinstatement. (d-g) Line graphs: 2-minute light OFF  
565 and ON epochs during Recall for the two experimental ArchT groups (DG Exp & BLA Exp) and  
566 the two control no-opsin groups (DG eYFP & BLA eYFP). Bar graphs: Quantification of  
567 average freezing between light OFF vs. light ON epochs for each group. (d) DG Exp Recall ( $t_{24}$   
568 = 2.781, \* $P = 0.0104$ ; paired t-test;  $n = 25$  paired epochs from 13 mice). (e) BLA EXP Recall ( $t_{17}$   
569 = 4.277, \*\*\* $P = 0.0005$ ; paired t-test;  $n = 18$  paired epochs from 9 mice). (f) DG eYFP Recall  
570 ( $t_{21} = 0.05067$ , n.s.,  $P = 0.9600$ ; paired t-test;  $n = 22$  paired epochs from 11 mice). (g) BLA eYFP  
571 Recall ( $t_{15} = 0.3915$ , n.s.,  $P = 0.7010$ ; paired t-test;  $n = 16$  paired epochs from 8 mice). (h)  
572 Behavioral schedule to test for specificity of DG and BLA fear ensemble in disrupting  
573 reinstatement-induced fear. Mice had cells active during Female Exposure labeled in either the  
574 DG or BLA, and then underwent FC, EXT, Shock Reinstatement, and had the labeled cells  
575 inhibited during Recall. (i,j) Same line and bar graphs as in d-g, but for the behavioral design in  
576 h. (i) DG Pos Recall ( $t_{23} = 2.053$ , n.s.,  $P = 0.0516$ ; paired t-test;  $n = 24$  paired epochs from 12  
577 mice). (j) BLA Pos Recall ( $t_{15} = 0.1986$ , n.s.,  $P = 0.8452$ ; paired t-test;  $n = 16$  paired epochs from  
578 8 mice). (k) Freezing difference scores across the three DG groups (Exp, Pos, eYFP), calculated  
579 as freezing in light ON epoch – freezing in light OFF epoch, for each set of epochs for each  
580 mouse. There was a strong trend towards a decrease in freezing in the light ON epoch in the Exp  
581 group vs. the eYFP group, and there was no difference in the Pos vs. eYFP groups (from left to  
582 right:  $n = 25$  scores from 13 mice, 24 scores from 12 mice, 22 scores from 11 mice;  $F_{2,68} = 2.351$ ,  
583  $P = 0.1030$ ; DG Exp vs. DG eYFP, n.s.,  $P = 0.0658$ ; DG Pos vs. DG eYFP, n.s.,  $P = 0.2682$ ; one-  
584 way ANOVA followed by Dunnett's test). (l) Same as k but for BLA groups. The BLA Exp  
585 group showed significantly lower freezing during the light ON epoch compared to the BLA  
586 eYFP group ( $p = 0.0122$ ), whereas there was no difference in the BLA Pos vs. BLA eYFP  
587 groups ( $p = 0.8797$ ) (from left to right:  $n = 18$  scores from 9 mice, 16 scores from 8 mice, 16  
588 scores from 8 mice;  $F_{2,47} = 4.811$ ,  $P = 0.0126$ ; BLA Exp vs. BLA eYFP, \* $P = 0.0122$ ; BLA Pos  
589 vs. BLA eYFP, n.s.,  $P = 0.8797$ ; one-way ANOVA followed by Dunnett's test). (m) Summary  
590 graph of freezing difference scores across all groups in Figure 3. While mice in the BLA and DG  
591 Exp groups show significantly less freezing during light ON epochs, the BLA and DG Pos  
592 groups and BLA and DG eYFP groups show no difference in freezing between light ON and  
593 light OFF epochs (from left to right:  $n = 18$  scores from 9 mice, 25 scores from 13 mice, 16  
594 scores from 8 mice, 24 scores from 12 mice, 16 scores from 8 mice, 22 scores from 12 mice;

595 BLA Exp,  $t_{17} = 4.277$ , \*\*\* $P = 0.0005$ ; DG Exp,  $t_{24} = 2.781$ , \* $P = 0.0104$ ; BLA Pos,  $t_{15} = 0.1986$ ,  
596 n.s.,  $P = 0.8452$ ; DG Pos,  $t_{23} = 2.053$ , n.s.,  $P = 0.0516$ ; BLA eYFP,  $t_{15} = 0.3915$ , n.s.,  $P = 0.7010$ ;  
597 DG eYFP,  $t_{21} = 0.05076$ , n.s.,  $P = 0.9600$ ; one-sample t-tests,  $\mu_0 = 0$ ).  
598

599 **Figure 3 – figure supplement 1.** Inhibition of BLA fear ensemble does not prevent  
600 reinstatement. **(a)** Schematic of viral strategy. A viral cocktail of AAV9-c-Fos-tTA and AAV9-  
601 TRE-ArchT-eYFP was infused into the BLA for activity-dependent induction of ArchT-eYFP.  
602 **(b)** Representative microscope image of BLA injection site. Dotted line indicates optic fiber  
603 placement. **(c)** Behavioral schedule to test if inhibition of BLA fear ensemble during Shock  
604 Reinstatement can prevent reinstatement. **(d)** Left: Freezing during fear conditioning and  
605 extinction. Upper right: Compared to the first 3 minutes of FC (baseline freezing), mice froze  
606 significantly more in the first three minutes of the EXT1 session ( $t_{10} = 17.112$ , \*\*\* $P < 0.0001$ ;  
607 paired t-test;  $n = 10$  mice). Bottom right: Mice spent significantly less time freezing in the last  
608 three minutes of EXT2 as compared to the first three minutes of EXT1 ( $t_{10} = 5.5159$ , \*\*\* $P =$   
609 0.0003; paired t-test;  $n = 10$  mice). **(e)** Compared to no-opsin controls (eYFP group),  
610 experimental mice that received optical inhibition (ArchT group) showed comparable levels of  
611 freezing during Recall, indicating that inhibition of the BLA fear ensemble did not prevent  
612 reinstatement ( $t_9 = 0.935$ , n.s.,  $P = 3742$ ; unpaired t-test; ArchT,  $n = 7$  mice; eYFP,  $n = 4$  mice).  
613

614 **Figure 3 – figure supplement 2.** Stimulation of BLA or DG fear ensemble does not mimic  
615 reinstatement. **(a)** Behavioral schedule to test if stimulation of BLA fear ensemble in a novel  
616 environment can mimic reinstatement. **(b)** Left: Freezing during fear conditioning and extinction  
617 for BLA-implanted animals. Middle: Compared to the first 3 minutes of FC (baseline freezing),  
618 mice froze significantly more in the first three minutes of the EXT1 session ( $t_{15} = 17.171$ , \*\*\* $P <$   
619 0.0001; paired t-test;  $n = 16$  mice). Right: Mice spent significantly less time freezing in the last  
620 three minutes of EXT2 as compared to the first three minutes of EXT1 ( $t_{15} = 7.9973$ , \*\*\* $P <$   
621 0.0001; paired t-test;  $n = 16$  mice). **(c)** Left: Freezing during fear conditioning and extinction for  
622 DG-implanted animals. Middle: Compared to the first 3 minutes of FC (baseline freezing), mice  
623 froze significantly more in the first three minutes of the EXT1 session ( $t_{15} = 13.238$ , \*\*\* $P <$   
624 0.0001; paired t-test;  $n = 16$  mice). Right: Mice spent significantly less time freezing in the last  
625 three minutes of EXT2 as compared to the first three minutes of EXT1 ( $t_{15} = 5.9671$ , \*\*\* $P <$   
626 0.0001; paired t-test;  $n = 16$  mice). **(d)** Left: Freezing across Recall session after BLA fear  
627 ensemble stimulation for ChR2 and eYFP groups. Right: Comparison of average freezing during  
628 Recall session after BLA fear ensemble stimulation, for ChR2 and eYFP groups ( $t_{14} = 0.8265$ ,  
629 n.s.,  $P = 0.4224$ ; unpaired t-test;  $n = 8$  mice in each group). **(e)** Left: Freezing across Recall  
630 session after DG fear ensemble stimulation for ChR2 and eYFP groups. Comparison of average  
631 freezing during Recall session after DG fear ensemble stimulation, for ChR2 and eYFP groups  
632 ( $t_{14} = 1.522$ , n.s.,  $P = 0.1503$ ; unpaired t-test;  $n = 8$  mice in each group).  
633

634 **Figure 3 – figure supplement 3.** Inhibition of the fear ensemble after extinction does not alter  
635 freezing behavior. **(a)** Behavioral design. Mice underwent FC and two EXT sessions, followed  
636 by an 8-minute Recall session, with 2-minute light OFF/light ON epochs. **(b)** Left: Freezing  
637 during fear conditioning and extinction. Middle: Compared to the first 3 minutes of FC (baseline  
638 freezing), mice froze significantly more in the first three minutes of the EXT1 session ( $t_{15} =$   
639 25.898, \*\*\* $P < 0.0001$ ; paired t-test;  $n = 16$  mice). Right: Mice spent significantly less time  
640 freezing in the last three minutes of EXT2 as compared to the first three minutes of EXT1 ( $t_{15} =$

641 9.7348, \*\*\*\*P < 0.0001; paired t-test; n = 16 mice). (c-e) Line graphs: 2-minute light OFF and  
642 ON epochs during Recall for the two experimental ArchT groups (DG ArchT & BLA ArchT)  
643 and the one control no-opsin group (DG eYFP). Bar graphs: Quantification of average freezing  
644 between light OFF vs. light ON epochs for each group. (c) DG ArchT Recall ( $t_{11} = 1.65$ , n.s., P =  
645 0.1273; paired t-test; n = 12 paired epochs from 6 mice). (d) DG eYFP Recall ( $t_7 = 0.4724$ , n.s.,  
646 P = 0.6510; paired t-test; n = 8 paired epochs from 4 mice). (e) BLA ArchT Recall ( $t_{11} = 0.9078$ ,  
647 n.s., P = 0.3835; paired t-test; n = 12 paired epochs from 6 mice). (f) Summary graph of freezing  
648 difference scores across all graphs in this figure, calculated as freezing in light ON epoch –  
649 freezing in light OFF epoch, for each set of epochs for each mouse. There was no significant  
650 difference in freezing between the DG ArchT and DG eYFP groups ( $t_{18} = 0.8689$ , n.s., P =  
651 0.3963; unpaired t-test; DG ArchT, n = 12 scores from 6 mice; DG eYFP, n = 8 scores from 4  
652 mice).

653

654

655

656

657

658

659

660

661

662

663

664

665

666

667

668

669

670

671

672

673

674

675

676

677

678

679

680

681

682

683

684

685

686

687 **Methods**

688

689 Subjects

690 Wildtype male C57BL/6 mice (6-8 weeks of age; Charles River Labs) were housed in  
691 groups of 4-5 mice per cage. The animal facilities (vivarium and behavioral testing rooms) were  
692 maintained on a 12:12-hour light cycle (lights on at 0700). Mice were placed on a diet containing  
693 40 mg/kg doxycycline (Dox) for a minimum of two days before receiving surgery with access to  
694 food and water *ad libitum*. Mice recovered for at least ten days after surgery. Dox-containing diet  
695 was replaced with standard mouse chow (*ad libitum*) 48 hours prior to behavioral tagging to  
696 open a time window of activity-dependent labeling (Ramirez et al., 2013).

697 All procedures relating to mouse care and treatment conformed to the institutional and  
698 National Institutes of Health guidelines for the Care and Use of Laboratory Animals. No  
699 statistical methods were used to predetermine sample size; however, sample sizes were chosen  
700 based on sample sizes in previous studies (Ramirez et al., 2013). Data collection and analysis  
701 were not performed blind to the conditions of the experiments.

702

703 Activity-dependent viral constructs

704 pAAV<sub>9</sub>-cFos-tTA, pAAV<sub>9</sub>-TRE-eYFP, and pAAV<sub>9</sub>-TRE-ArchT-eYFP were constructed as  
705 previously described (Ramirez et al., 2015). pAAV<sub>9</sub>-c-Fos-tTA was combined with pAAV<sub>9</sub>-TRE-  
706 eYFP or pAAV<sub>9</sub>-TRE-ArchT-eYFP prior to injection at a 1:1 ratio.

707

708 Stereotaxic surgeries

709 *Opsin injections and optic fiber implants:* Stereotaxic injections and optical fiber  
710 implants followed methods previously reported (Ramirez et al., 2015). All surgeries were  
711 performed under stereotaxic guidance and subsequent coordinates are given relative to Bregma  
712 (in mm). Mice were mounted into a stereotaxic frame (Kopf Instruments, Tujunga, CA, USA)  
713 and anesthetized with 3% isoflurane during induction and lowered to 1-2% to maintain  
714 anesthesia (oxygen 1L/min) throughout the surgery. Ophthalmic ointment was applied to both  
715 eyes to prevent corneal desiccation. Hair was removed with scissors and the surgical site was  
716 cleaned with ethanol and betadine. Following this, an incision was made to expose the skull.  
717 Bilateral craniotomies involved drilling windows through the skull above the injection sites using  
718 a 0.5 mm diameter drill bit. Coordinates were -1.35mm anteroposterior (AP), ±3.45mm  
719 mediolateral (ML), and -5.15mm dorsoventral (DV) for basolateral amygdala (BLA) (Davis et  
720 al., 2017); and -2.2mm AP, ±1.3mm ML, and -2.0mm DV for dorsal dentate gyrus  
721 (dDG) (Ramirez et al., 2015). All mice were injected with a volume of 0.3 µl of AAV9 cocktail  
722 per site at a control rate of 0.1 µl min<sup>-1</sup> using a mineral oil-filled 33-gage beveled needle attached  
723 to a 10 µl Hamilton microsyringe (701LT; Hamilton) in a microsyringe pump (UMP3; WPI).  
724 The needle remained at the target site for two minutes post-injection before removal. For dDG  
725 optogenetic experiments, a bilateral optic fiber implant (200 µm core diameter; Doric Lenses)  
726 was chronically implanted above the injection site (-1.6mm DV). For BLA optogenetic  
727 experiments, monofibers were implanted above each injection site (-4.9mm DV). Jewelry screws  
728 secured to the skull acted as anchors. Layers of adhesive cement (C&B Metabond) followed by  
729 dental cement (A-M Systems) were spread over the surgical site. Mice that did not receive  
730 implants had their incision sutured. Mice received 0.1 mL of 0.3 mg/ml buprenorphine  
731 (intraperitoneally) following surgery and were placed on a heating pad during recovery.

732        *GCaMP6f injections and lens implants:* Mice in Ca<sup>2+</sup> imaging experiments underwent  
733 three separate serial surgeries. First, mice received unilateral infusions of AAV9-Syn-GCaMP6f  
734 (U Penn Vector Core) into either right CA1 (AP -2.0 mm, ML +1.5 mm, DV -1.5 mm) or right  
735 BLA (AP -1.35 mm, ML +3.45 mm, DV -5.05 mm). The viral vector was injected at a rate of 40  
736 nL/min and allowed 10 min to diffuse before the scalp was sutured.

737        Two to four weeks after viral infusion, mice were implanted with a gradient index  
738 (GRIN) lens into either CA1 (1 mm diameter, 4 mm length, Inscopix; AP -2.25 mm, ML +1.8  
739 mm, DV -1.3 mm) or BLA (0.65 mm diameter, 7.3 mm length; AP -1.25 mm, ML +3.15 mm,  
740 DV -4.85 mm). For CA1 implants, overlying neocortex was aspirated under continuous irrigation  
741 with cold 0.9% saline until vertical white fibers were visible (Resendez et al., 2016). For BLA  
742 implants, a tract was created using a stereotactically lowered 27-gauge needle (0.5 mm diameter)  
743 into the craniotomy prior to insertion of the lens. Gaps between the lens and the skull were filled  
744 using Kwik-Sil (World Precision Instruments) and the lens was then adhered to the skull using  
745 Metabond. The surface of the lens was covered with a protective cap made of Kwik-Cast (World  
746 Precision Instruments) until base plate attachment.

747        Finally, one week after the lens implant, mice were implanted with a base plate for  
748 microscope attachment. A plastic base plate was magnetically attached to the bottom of the  
749 microscope. The microscope objective was then aligned to the GRIN lens and lowered until cells  
750 came into focus, as observed via nVista recording software (Inscopix). The base plate was then  
751 adhered to the surrounding Metabond on the animal's skull using a dental composite (Flow-It  
752 ALC, Pentron) and strengthened with an additional layer of Metabond.

753        Histological assessment verified viral targeting and fiber/lens placement. Data from off-  
754 target injections and implants were not included in analyses.

#### 755        Optogenetic methods

756        Optic fiber implants were plugged into a patch cord connected to a 520nm green laser  
757 diode controlled by automated software (Doric Lenses). Laser diode output was tested at the  
758 beginning of every experiment to ensure that at least 10 mW of power was delivered at the end  
759 of the optic fiber tip (Doric lenses). Mice began the stimulation trial with a 2-min light-off epoch,  
760 followed by 2-min optical stimulation (15 ms pulse width, 20 Hz), and then repeated, such that  
761 the mice underwent a light-OFF/ON/OFF/ON pattern for a total of 8-min.

#### 762        Behavioral tagging

763        Dox diet was replaced with standard lab chow (*ad libitum*) 48-hours prior to behavioral  
764 tagging. *Female exposure:* One female mouse (PD 30-40) was placed into a clean home cage  
765 with a clear cage top, which was used as the interaction chamber. The experimental male mouse  
766 was then placed into the chamber and allowed to interact freely for one hour(Ramirez et al.,  
767 2015). *Fear conditioning:* Mice were placed into a conditioning chamber and received fear  
768 conditioning (see below) over a 500-second training session (including exposure to four 1.5 mA  
769 foot shocks). Following behavioral tagging, the male mouse was returned to their home cage  
770 with access to Dox diet (Ramirez et al., 2013).

#### 771        Behavior

772        All behavior assays were conducted during the light cycle of the day (0730–1930). Mice  
773 were handled for 1-2 days, 2 min per day, before all behavioral experiments, and were run by  
774 cage. The entire behavioral schedule includes female exposure, fear conditioning, extinction,

778 reinstatement, and recall (described below). Which of these behaviors the mice underwent  
779 depended on the experiment.

780 *Female exposure:* One female mouse (PD 30-40) was placed into a clean home cage with  
781 a clear cage top and no bedding, which was used as the interaction chamber. The experimental  
782 male mouse was then placed into the chamber and allowed to interact freely for one  
783 hour(Ramirez et al., 2015).

784 *Fear conditioning:* Fear conditioning occurred in one of four mouse conditioning  
785 chambers (Coulbourn Instruments, Whitehall, PA, USA) with metal-panel side walls, Plexiglas  
786 front and rear walls, and a stainless-steel grid floor composed of 16 grid bars. The grid floor was  
787 connected to a precision animal shocker (Coulbourn Instruments, Whitehall, PA, USA) set to  
788 deliver a 2-second 1.5 mA foot shock unconditioned stimulus (US). A ceiling-mounted video  
789 camera recorded activity and fed into a computer running FreezeFrame3 software (Actimetrics,  
790 Wilmette, IL, USA). The software controlled stimuli presentations and recorded videos from  
791 four chambers simultaneously. The program determined movement as changes in pixel  
792 luminance. Context alterations included changes to spatial, olfactory, tactile, and lighting cues.  
793 The conditioning chamber with room lights off was designated as Context A. Context B involved  
794 modifications to the conditioning chamber, including vertical black and white strips spaced ~ 3  
795 cm apart obscuring the front and rear walls, black inserts placed between grids to slightly alter  
796 dimensions of the box, 1 mL of almond extract in a plastic container positioned below the grid  
797 floor, and room lights on. Context C also involved modifications to the conditioning chamber,  
798 with a plastic sheet with a cross-hatch texture placed over the shock grid to change tactile cues, a  
799 black sheet obscuring the front walls, 1 mL of orange extract in a plastic container position  
800 below the grid floor, and room lights on. The chambers were cleaned with 70% ethanol solution  
801 prior to animal placement. Contextual fear conditioning occurred in Context A. Briefly, mice  
802 were placed into the conditioning context for a 500-second acquisition session, including a 180-  
803 second baseline period followed four 1.5 mA, 2-second foot shock USs (interstimulus interval  
804 [ISI] equals 80-sec). In optogenetic experiments, mice had patch cords attached near the  
805 conditioning chamber by the experimenter, and were run two mice at a time.

806 Fear conditioning data are collected using FreezeFrame3 software (Actimetrics, Wilmette  
807 IL) with the bout length set at 1.25-sec and the freezing threshold initially set as described in the  
808 program instructions. Freezing is defined as changes in pixel luminance falling below a  
809 threshold. An experimenter adjusted the threshold so that freezing behavior involves the absence  
810 of all movement except those needed for respiration as previously described. Freezing behavior  
811 was scored as the percentage of time spent freezing during a given bout of time. Statistical  
812 analyses involved paired t-tests comparing within subject differences (i.e. light off vs light on  
813 epochs), unpaired t-tests comparing across experimental groups (e.g. ArchT group vs. eYFP  
814 group), and one-sample t-tests comparing freezing differences scores to a  $\mu_0 = 0$ .

815 *Extinction:* Extinction occurred in Context A (described above) the day following fear  
816 conditioning. Mice were placed in Context A for 30-min sessions once per day, for two days. As  
817 in fear conditioning, cages of four mice were run simultaneously, and cages of five mice were  
818 run as three mice first, then the remaining two.

819 *Reinstatement:* Reinstatement occurred in Context B (described above) the day following  
820 the second day of extinction. Mice were placed in Context B and given a 1.5 mA, 2-second foot  
821 shock 1-second into the trial. Mice were left in the chamber for another 60-seconds before being  
822 removed. As opposed to being run four mice simultaneously as in fear conditioning and  
823 extinction, each mouse in a cage was run individually for reinstatement.

824        *Recall:* Recall for behavioral and overlap experiments involved placement in a context  
825 for 5-min. In this case, as in fear conditioning and extinction, cages of four mice were run  
826 simultaneously while cages of five mice were run as three mice first, then the remaining two. In  
827 optogenetic experiments, recall involved an 8-min session consisting of 2-min epochs of  
828 alternating light off and light on. In this case, mice were run one or two at a time.  
829

830        Immunohistochemistry.

831        Mice were anesthetized with 3% isoflurane and perfused transcardially with cold (4° C)  
832 phosphate- buffered saline (PBS) followed by cold 4% paraformaldehyde (PFA) in PBS. Brains  
833 were extracted and stored overnight in PFA at 4°C. Fifty µm coronal sections were collected in  
834 serial order using a vibratome and collected in cold PBS (100 µm coronal sections were collected  
835 when solely verifying injection site and implant placement). Immunostaining involved washing  
836 sections in PBS with 0.2% triton (PBST) for 10-minutes (x3). Sections were blocked for 1 hour  
837 at room temperature in PBST and 5% normal goat serum (NGS) on a shaker. Sections were  
838 transferred to wells containing primary antibodies (1:5000 rabbit anti-c-Fos [SySy]; 1:500  
839 chicken anti-GFP [Invitrogen]) and allowed to incubate on a shaker overnight at 4°C. Sections  
840 were then washed in PBST for 10-min (x3), followed by 2-hour incubation with secondary  
841 antibody (1:200 Alexa 555 anti-rabbit [Invitrogen]; 1:200 Alexa 488 anti-chicken [Invitrogen]).  
842 Following three additional 10-min washes in PBST, sections were mounted onto micro slides  
843 (VWR International, LLC). Vectashield Hard Set Mounting Medium with DAPI (Vector  
844 Laboratories, Inc) was applied, slides were cover slipped, and allowed to dry overnight.  
845

846        Cell counting.

847        The number of eYFP- or cFos-immunoreactive neurons in the dentate gyrus and  
848 basolateral amygdala were counted to measure the number of active cells during defined  
849 behavioral tasks per mouse. Only animals that had accurate injections were selected for counting,  
850 and sections closest to the injection coordinates for each brain region were chosen (see the  
851 Stereotaxic surgeries section of Methods). All animals were sacrificed 90 minutes post-assay for  
852 immunohistochemical analyses. Fluorescence images were acquired using a confocal microscope  
853 (Zeiss LSM800, Germany) with a 10X objective for dentate gyrus images and 20X objective for  
854 basolateral amygdala images. Z-stacked images were taken at step sizes of 3µm for DG and  
855 1.54µm for BLA in the z-axis and maximum projections of these z-stacks were taken for  
856 counting.

857        For the dentate gyrus, the number of eYFP-positive and cFos-positive cells in a set region  
858 of interest were quantified manually using ImageJ. eYFP positive cells in the basolateral  
859 amygdala were quantified automatically using a custom Python script that detects cells based on  
860 size and circularity of objects in an image, while cFos-positive cells were quantified manually  
861 with ImageJ because of poorer signal to noise in cFos images compared with the eYFP images.

862        To calculate the percentage of re-activated cells we counted the number of eYFP-positive  
863 cells, cFos-positive cells, and both eYFP- and cFos-positive (Overlapped) cells. Re-activation  
864 was calculated as (Overlap/eYFP\*100). Overlap was compared across groups using unpaired t-  
865 test (two-groups) and one-way ANOVA (more than two groups). Relative expression of eYFP  
866 and cFos across groups was calculated as (#eYFP cells/Area) and (#cFos cell/Area) in arbitrary  
867 area units.

868

869        In vivo calcium imaging

870 A miniaturized microscope (Inscopix) was used to collect  $\text{Ca}^{2+}$  imaging videos in mice  
871 undergoing the fear reinstatement schedule. Videos were captured using nVista (Inscopix) at 20  
872 Hz in a 720 x 540 pixel field of view (1.1 microns/pixel). Microscope attachments were done  
873 while the mice were awake and restrained.

874  $\text{Ca}^{2+}$  imaging videos were cropped, spatially bandpass filtered, and motion corrected  
875 offline using Inscopix Data Processing Software v1.1. A  $\Delta\text{F/F}$  movie was computed using the  
876 mean fluorescence of the movie as the baseline and PCA/ICA was used for automated  
877 segmentation of cell masks (Mukamel, Nimmerjahn, & Schnitzer, 2009). PCA/ICA putative cell  
878 masks were each manually inspected to verify that cells were accurately captured with high  
879 fidelity. Cells across imaging sessions were aligned and registered to each other using the  
880 automated CellReg software in Matlab (Sheintuch et al., 2017).

881 Population vectors (PVs) were computed for the entirety of the CFC session by taking the  
882 average  $\text{Ca}^{2+}$  transient rate for each cell while the mouse was in the fear conditioning chamber.  
883 PVs for EXT1, EXT2, and Recall were defined as the average  $\text{Ca}^{2+}$  transient rate for each 30 s  
884 time bin while the mouse was in the chamber. As a measure of the similarity of the population to  
885 the CFC network state, Pearson correlations were performed between each 30 s PV to the CFC  
886 PV. As a control, we also performed correlations between PVs from a neutral context to the CFC  
887 PV. Only cells that were active for both sessions being correlated (CFC and either EXT1, EXT2,  
888 or Recall) were considered.

889 We used piecewise regressions to determine whether reinstatement increased PV  
890 correlations (to CFC) greater than would be expected from chance. For each mouse, we fit PV  
891 correlation coefficients using time as a predictor for the EXT sessions and the Recall session  
892 separately. Next, using the regression models obtained from the EXT session data, we predicted  
893 the PV correlation value that should be observed during the first time bin in Recall. Then we  
894 compared the predicted values to the actual values derived from the y-intercepts of the regression  
895 models on the Recall data.

896

## 897 Neuronal Ensembles

898 We characterized neuronal ensembles from  $\text{Ca}^{2+}$  transient activity and correlated their  
899 later activity during Recall to relapse-associated freezing. To extract neuronal ensembles, we  
900 used a PCA/ICA method that was previously published (Lopes-dos-Santos et al., 2013). This  
901 method is a source separation algorithm that is similar in principle to the PCA/ICA that was run  
902 on  $\text{Ca}^{2+}$  imaging movies earlier (Mukamel et al., 2009). However, rather than extracting neurons  
903 from pixel fluorescence, we are now extracting ensembles from traces. First,  $\text{Ca}^{2+}$  traces were z-  
904 score normalized. Then, principal components analysis (PCA) was used to reduce the  
905 dimensionality of the trace matrix and to compute eigenvalues corresponding to the variances  
906 along the reduced dimensions. To produce a surrogate dataset for determining significant  
907 eigenvalues, we circularly shuffled each neuron's  $\text{Ca}^{2+}$  trace vector and performed PCA on that  
908 shuffled data 1000 times. Next, significant ensembles were tallied based on eigenvalues  
909 exceeding a statistically defined threshold (eigenvalues must be  $> 99\%$  of all the eigenvalues  
910 computed from the PCA of the shuffled data). To extract statistically independent ensembles, an  
911 independent components analysis (ICA) was run on the trace matrix with the number of  
912 components specified by the number of statistically significant ensembles (eigenvalues). From  
913 this computation, each ensemble now has a corresponding "pattern" vector describing the weight  
914 of each neuron contributing to that ensemble. For each ensemble, a projection matrix was  
915 computed from the outer product of these pattern vectors with the identity of the matrix set to 0

916 (to ensure that more than one neuron was needed to trigger an ensemble activation). The  
917 projection matrix was multiplied with each observation (frame) of the trace matrix to obtain  
918 ensemble activation strength. Finally, an ensemble was considered to be significantly activated if  
919 it exceeded 2 standard deviations above its mean activation strength.

920 Ensembles were extracted individually for CFC, EXT1, and EXT2. Only neurons that  
921 were active between these sessions and Recall were considered. After ensembles were extracted,  
922 their activity strength during Recall was calculated and the proportion of significant activations  
923 was correlated with freezing.

924

#### 925 Data Analysis.

926 Data were analyzed using Inscopix nVista in conjunction with custom-made R, Python,  
927 and Matlab scripts. Data were analyzed using paired t-tests (two factors) or with one-way and  
928 repeated measures ANOVAs (more than two factors), Wilcoxon signed-rank tests, and Mann-  
929 Whitney U tests (two-tailed, corrected for multiple comparisons using false discovery rate  
930 adjustments). Post-hoc analyses (Tukey's) were used to characterize treatment and interaction  
931 effects, when statistically significant (alpha set at p<0.05, two-tailed).

# Figure 1

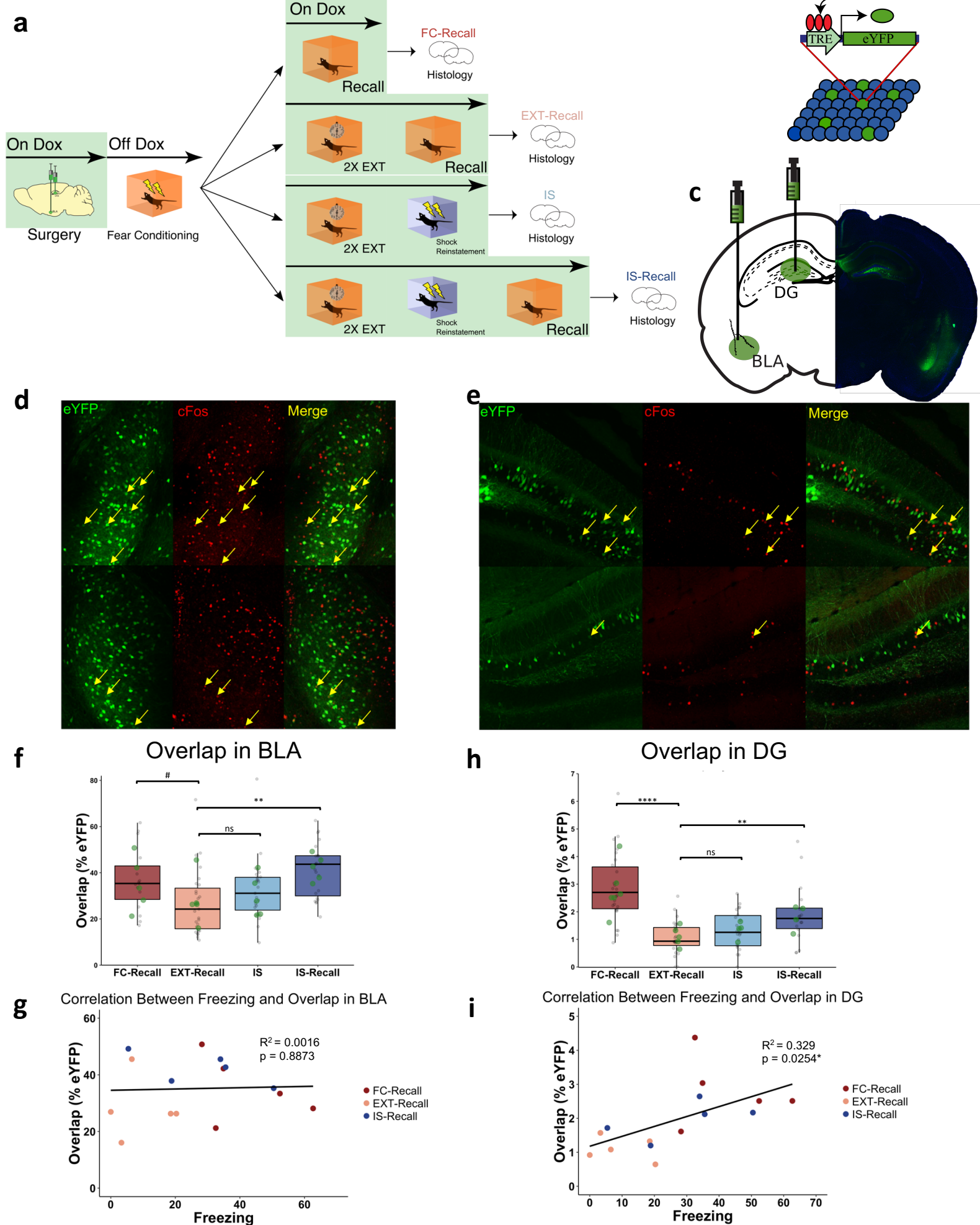


# Figure 1—figure supplement 1

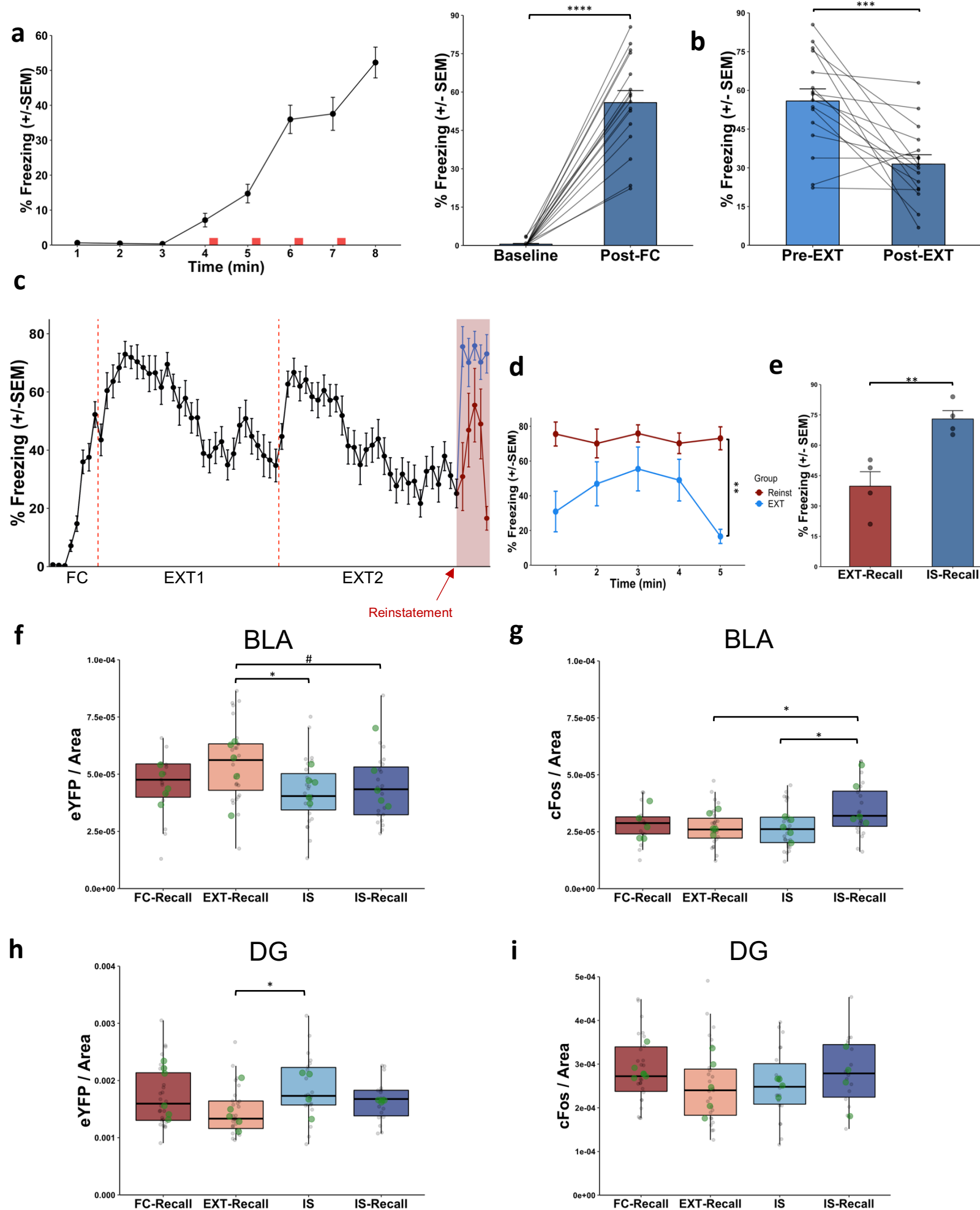


## Figure 1—figure supplement 2

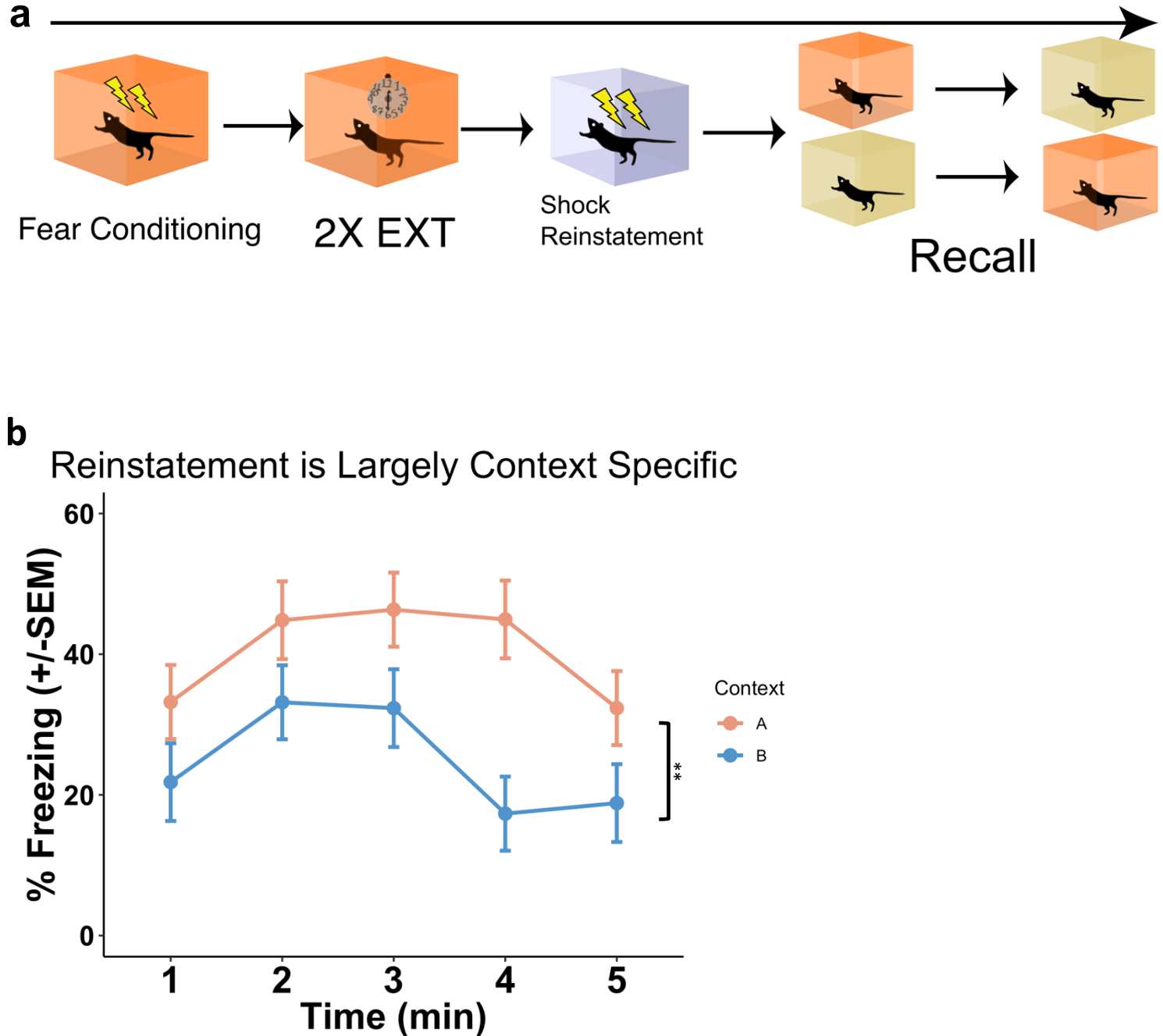


**Figure 2**

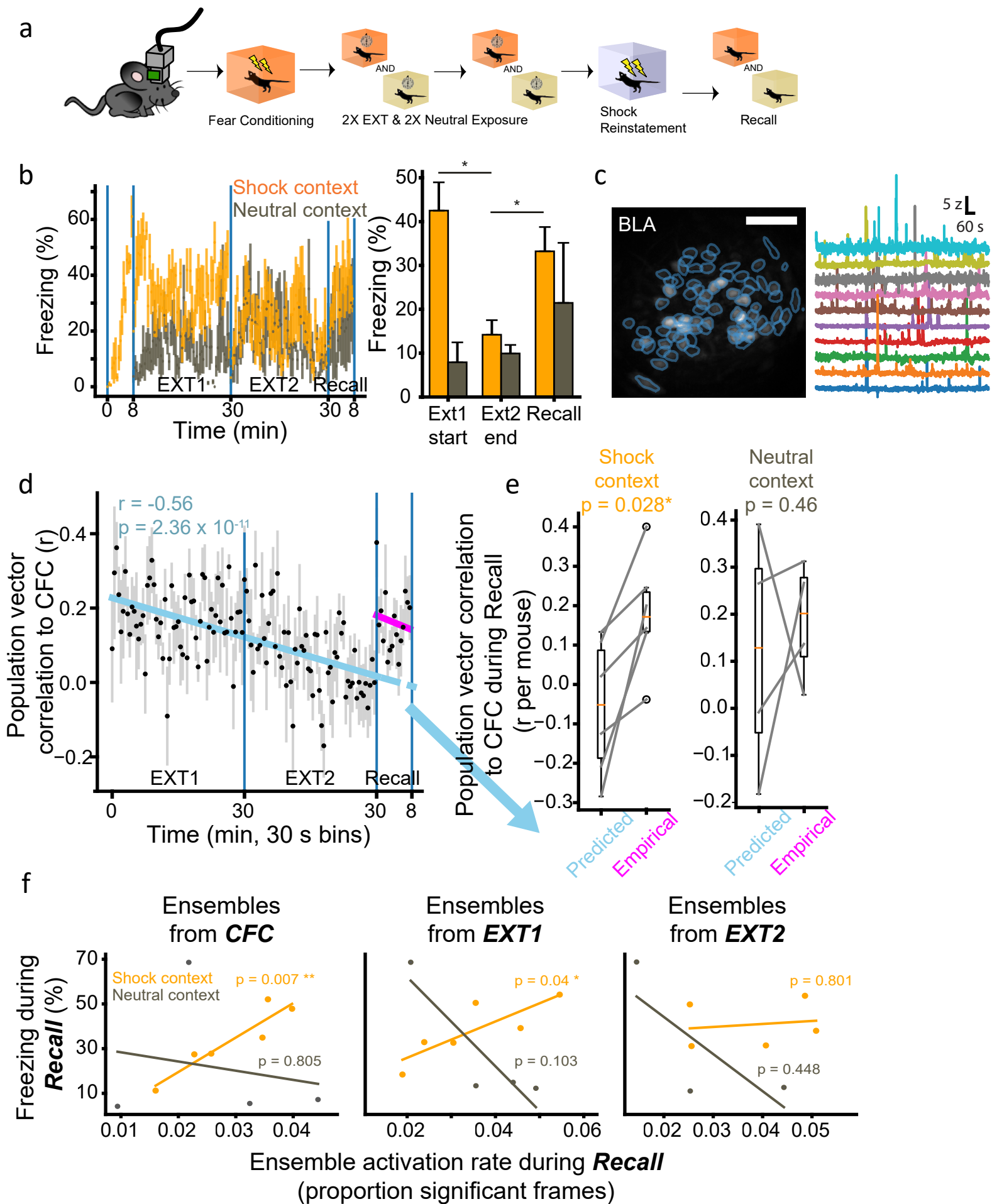
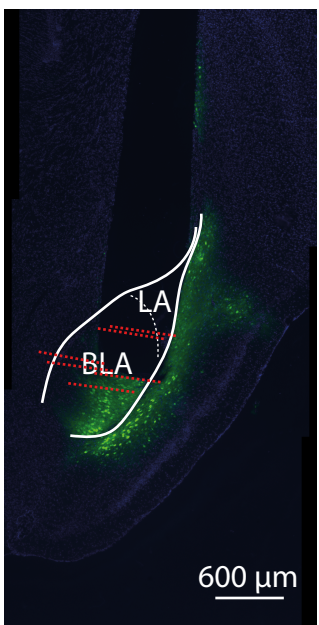
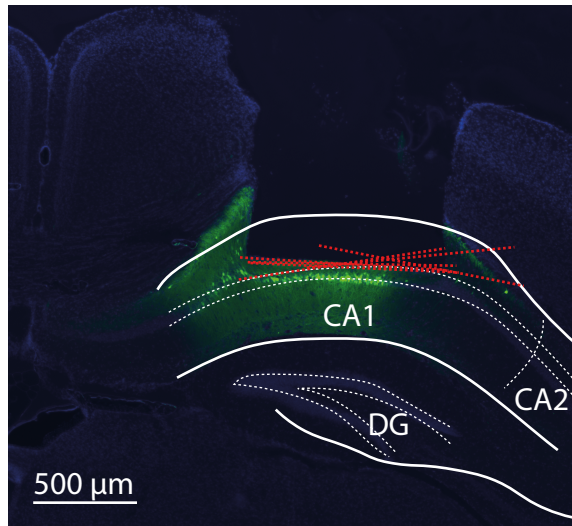


## Figure 2 - figure supplement 1

a

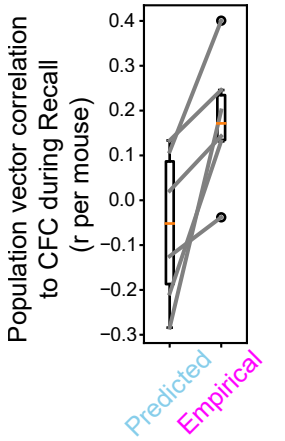
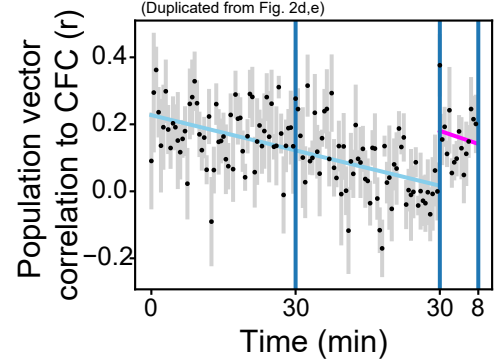


b

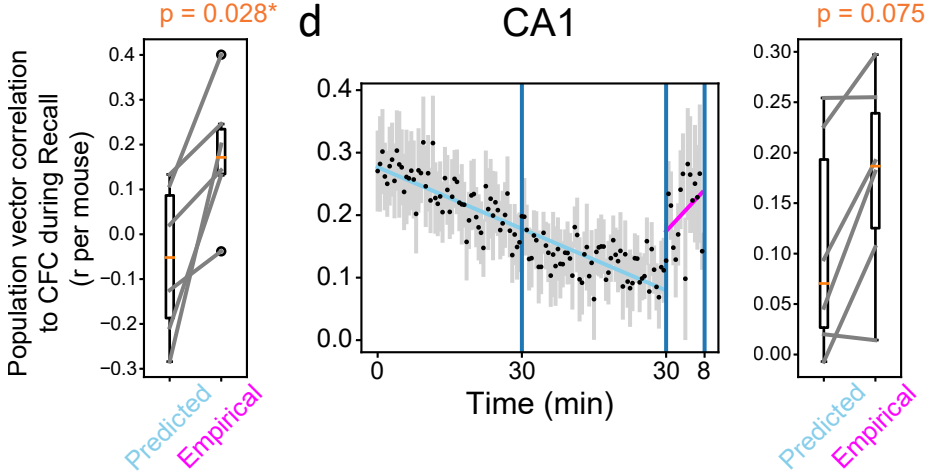


c

BLA



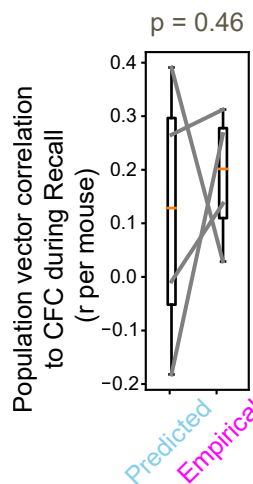
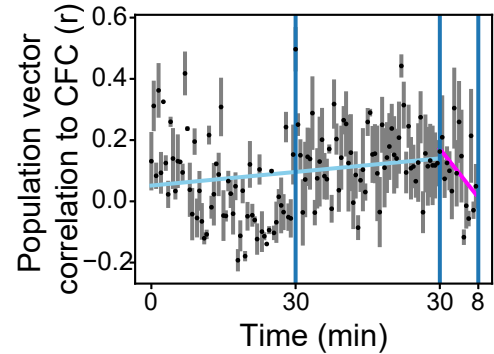
CA1



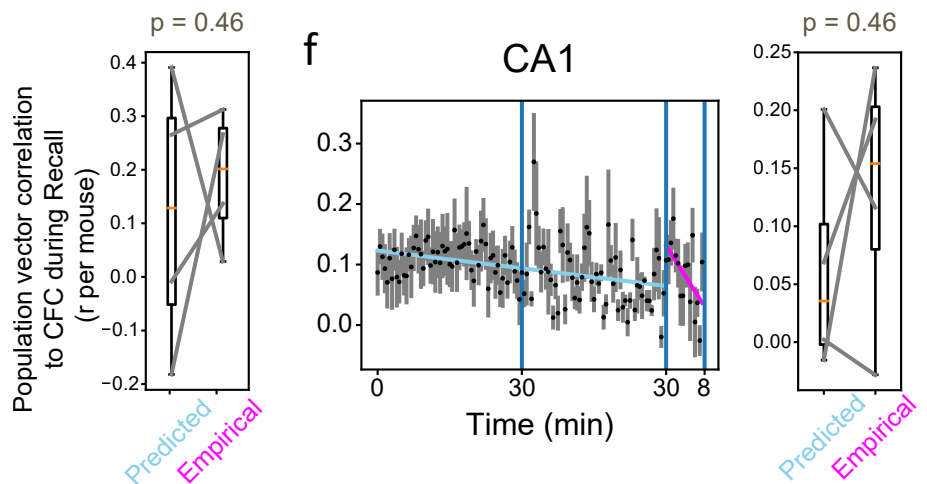
Shock context

e

BLA



CA1



Neutral context

## Figure 2 - figure supplement 2

a

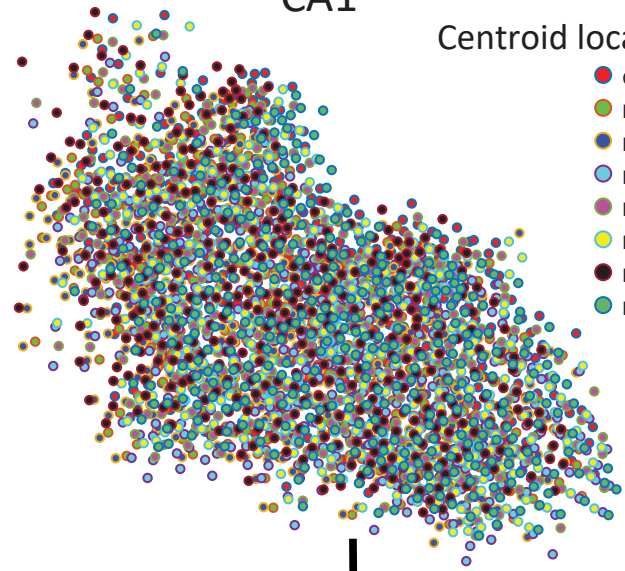
CA1

b

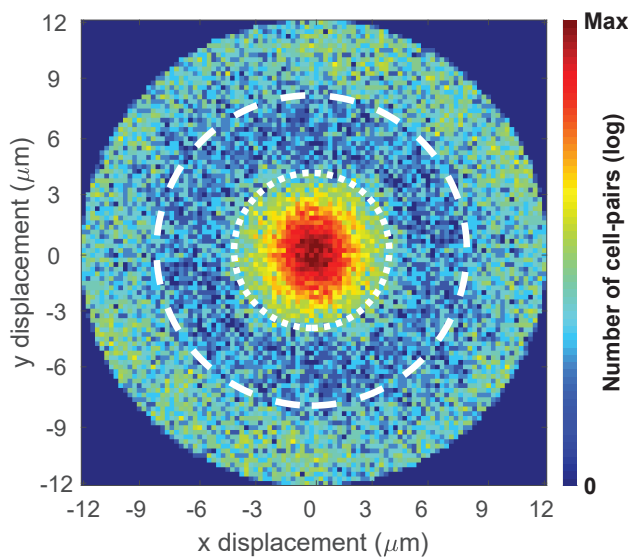
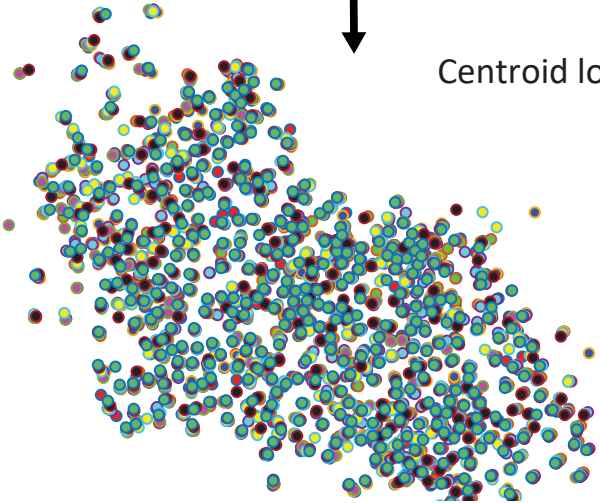
BLA

Centroid locations: Pre-alignment

- CFC
- EXT1, shock context
- EXT1, neutral context
- EXT2, neutral context
- EXT2, shock context
- Reinstatement
- Recall, shock context
- Recall, neutral context



Centroid locations: Post-alignment



b

BLA

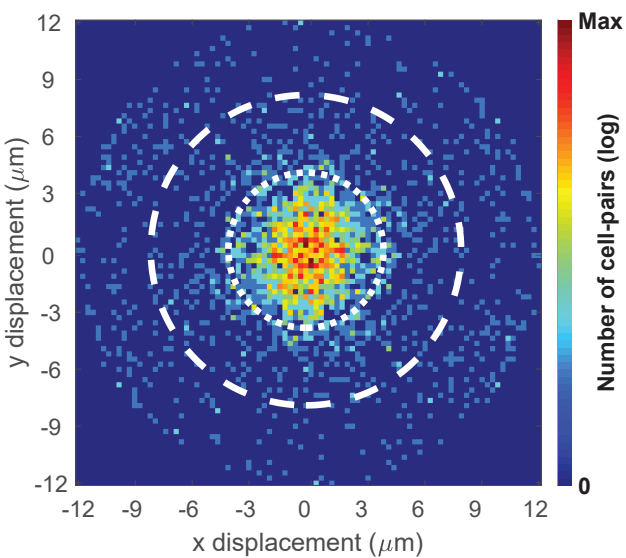
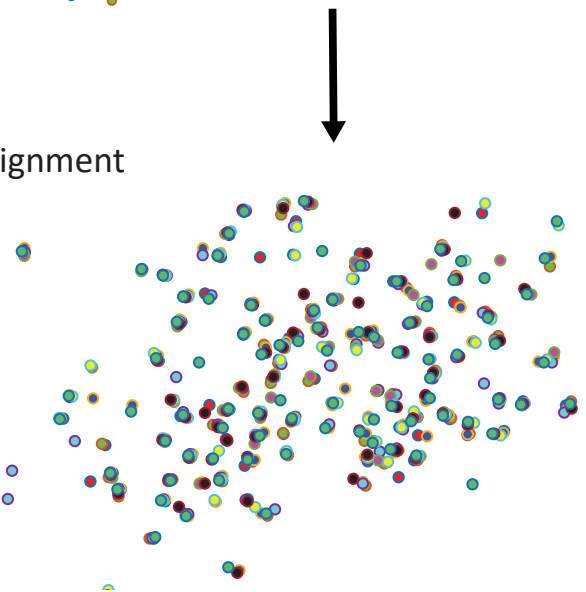
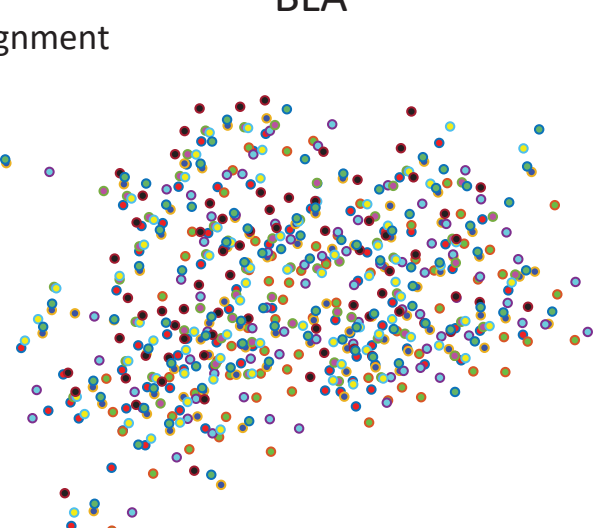


# Figure 3

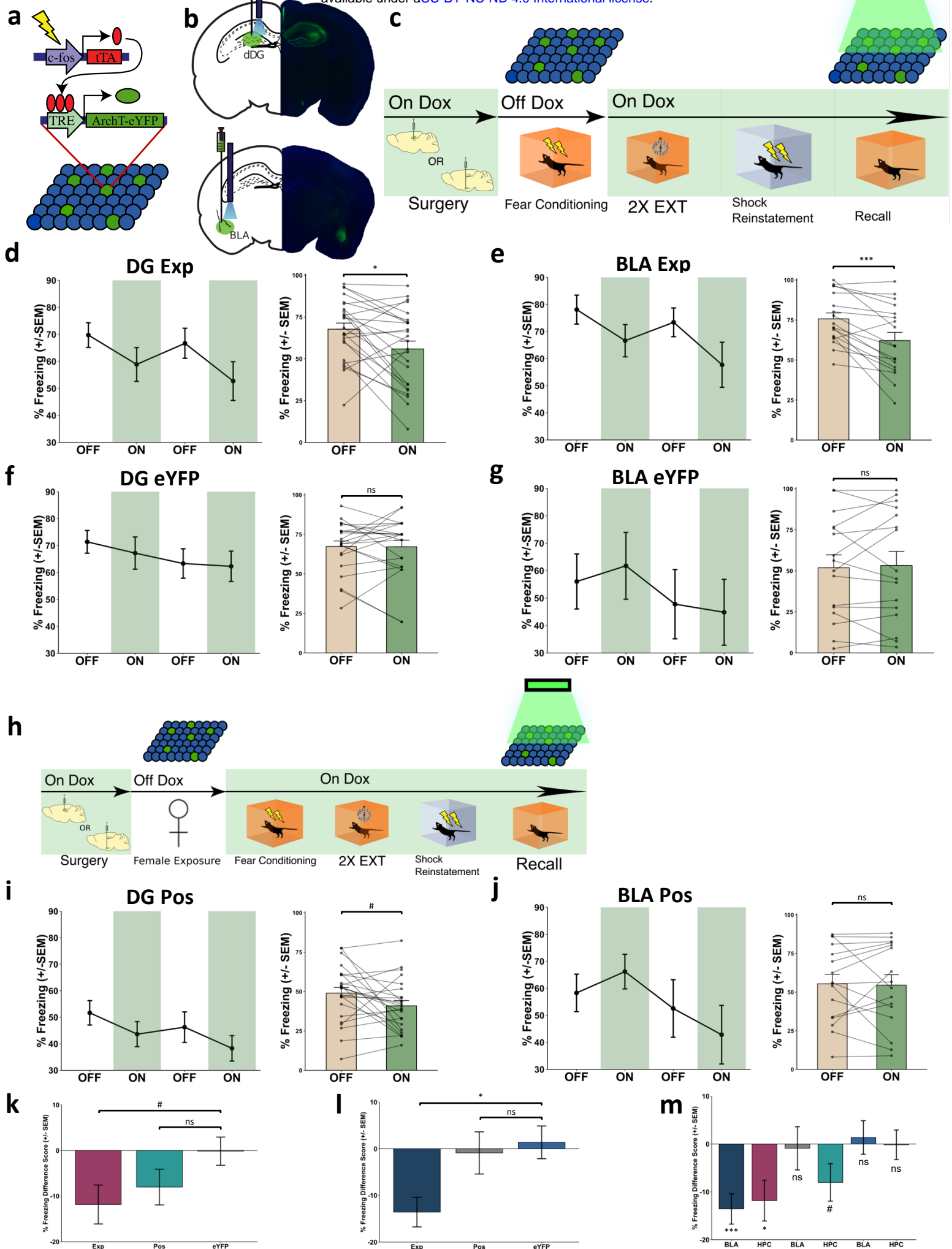
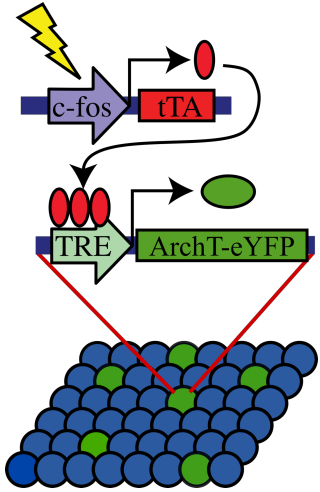
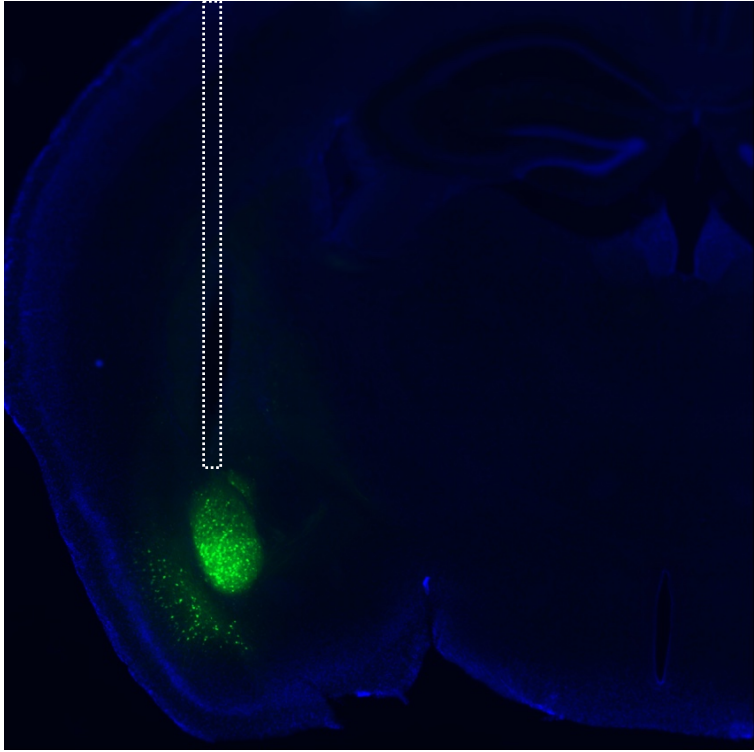


## Figure 3—figure supplement 1

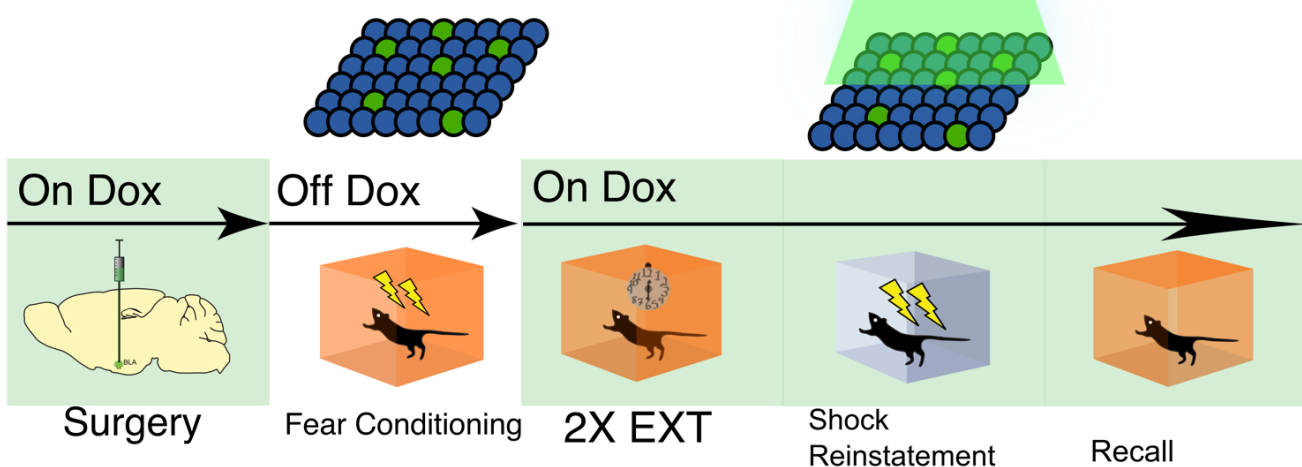
**a**



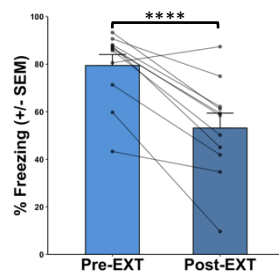
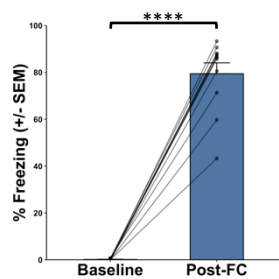
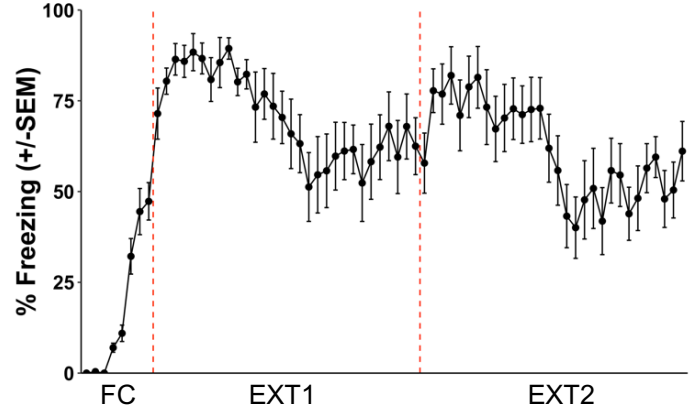
**b**



**c**



**d**



**e**

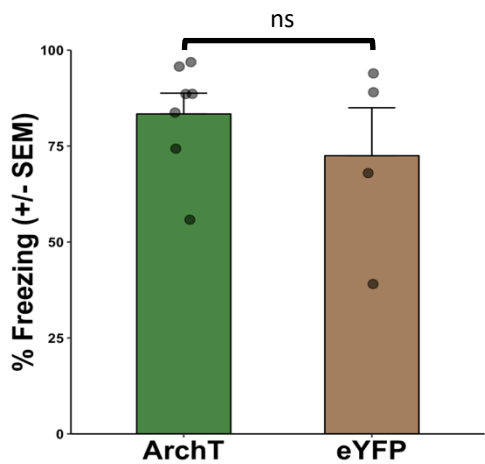
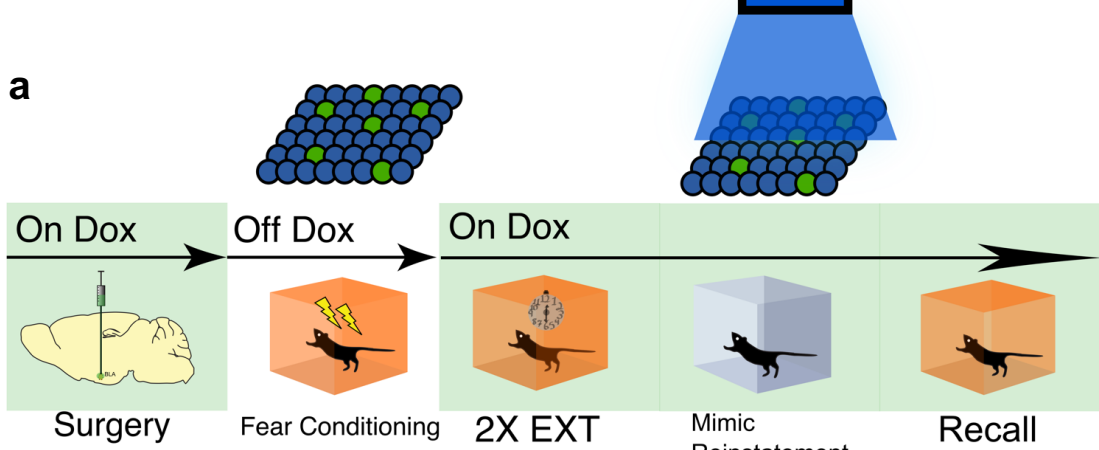
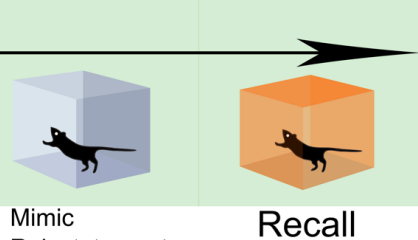
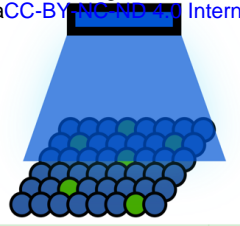
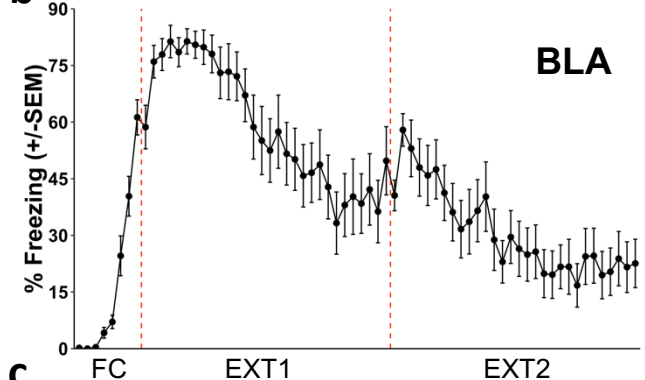


## Figure 3—figure supplement 2

**a**



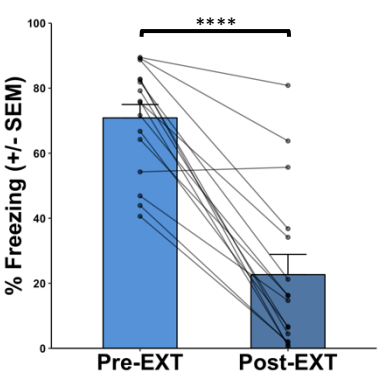
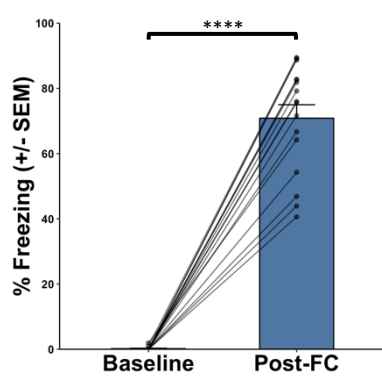
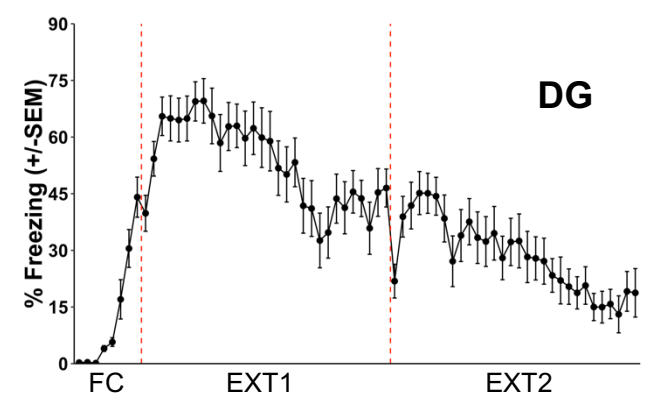
**b**



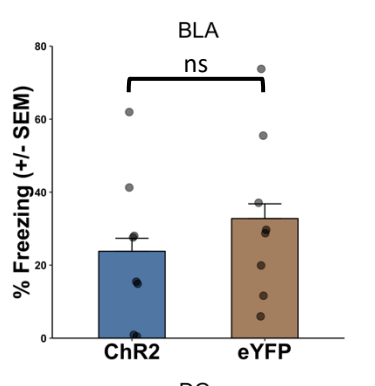
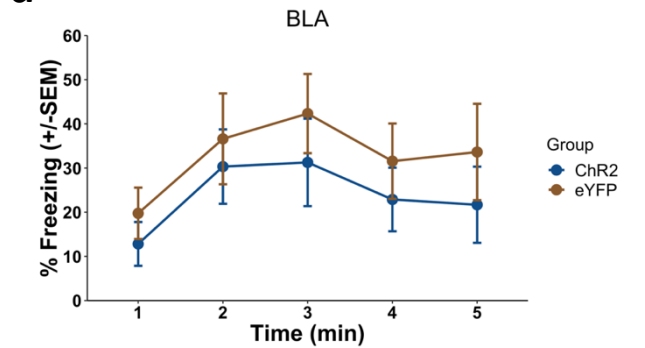
Mimic  
Reinforcement

Recall

**c**



**d**



**e**

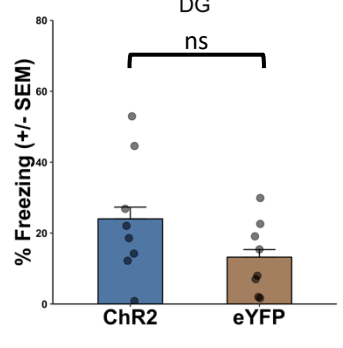
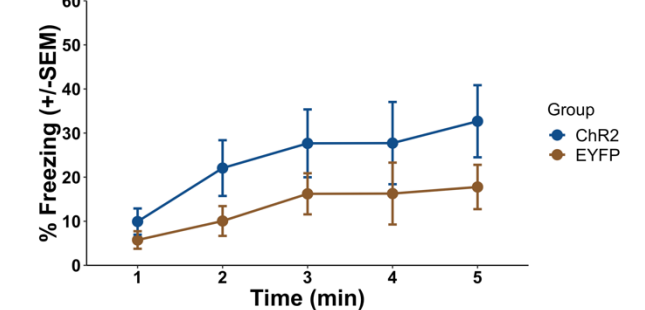


## Figure 3—figure supplement 3

